Photocatalytically active coatings for cement and air lime mortars: enhancement of the activity by incorporation of superplasticizers

M. Pérez-Nicolás[a], J. Plank[b], D. Ruiz-Izuriaga[a], I. Navarro-Blasco[a], J.M. Fernández[a], J.I. Alvarez[a]

[a]*Universidad de Navarra, Facultad de Ciencias, Departamento de Química, MIMED Research Group. Irunlarrea, 1. 31008 Pamplona, Spain*
[b]*Chair for Construction Chemistry, Department of Chemistry, TUM Center for Advanced PCE Studies, Technische Universität München, Lichtenbergstraße 4, Garching 85747, Germany*

Construction and Building Materials, 162 (2018) 628-648.
DOI: 10.1016/j.conbuildmat.2017.12.087

Abstract

Coatings made with water dispersions of different nano-particles of photocatalytic additives (titania and titania doped with iron and vanadium) were prepared with diverse superplasticizers, SPs, to optimize the atmospheric NO removal efficiency when applied onto cement- and air-lime mortars. The use of different polycarboxylate-based superplasticizers (52IPEG, 23APEG and 45PC6) prevented nano-particles from agglomeration. The steric hindrance, provided by a large density and length of side chains, was ascertained as the most effective repulsion mechanism and 52IPEG was the most efficient SP. In PC- and air-lime mortars, the coatings with polycarboxylate-based SPs improved the NO removal rates as compared with the SP-free coating: an average increase of NO degradation by 15% under UV and by 76% under solar light was found. This finding was related to the drop in the agglomeration of the photocatalysts, with more exposed active sites and a decrease of the electron-hole recombination rates. Capillary water absorption and water vapour permeability values showed that the coatings did not alter the performance of the mortars. SEM examination showed that the use of SPs enhanced the distribution of the photocatalysts yielding thinner coating layers and boosting the percolation of the active material within the mortars. Accelerated weathering showed a moderate reduction of NO removal efficiency. Coating with 52IPEG was the most efficient in preserving the activity. Measurements of Ti content showed a low washout of the TiO_2 nano-particles, supporting the long-run activity of these coatings.

Keywords: coating; NO removal; superplasticizer; photocatalysis; polycarboxylate

1. Introduction

Current urban environment presents some toxic gases as nitrogen oxides (NO and NO_2, usually noted as NO_x) which are responsible of air pollution. This polluted environment is a problem in our society because harmful gases and airborne particulate worsen human health [1]. Furthermore, the interaction of these compounds with the exposed areas of building materials has a direct detrimental effect on functionality and aesthetic building appearance [2], leading to dirt accumulation that demand spending economic resources in cleaning processes.

In order to decrease the levels of pollutants and, consequently, to reduce their negative impact, the photocatalytic oxidation (PCO) of these substances, their conversion into less or even non-harmful compounds and their final removal have shown to be efficient in different systems [3]. To this aim, building materials have to be modified either by inclusion of photocatalytic agents during their manufacture (bulk incorporation) or by *in situ* coating them with those active agents [4-7].

The excellent characteristics of TiO_2 among the photocatalysts have led to vast research on its applications. Different building materials, particularly cementing matrices, have been modified by the presence of TiO_2 [4-6]. Good values of gaseous pollutants removal together with the provision of self-cleaning ability to these active materials have been reported [6-8]. To tackle the well-known constricting sensitivity of the titania, which is limited to UV light, different dopant agents of the crystalline lattice of TiO_2 have been tested. Literature reports the use of many different metallic cations as well as p-block elements (individually or in co-doped systems) as dopant elements [9]. This approach reduces the band-gap of the titania lattice, allowing it to absorb visible light photons. Therefore, the photocatalytic compounds, with enlarged sensitivity, can be active under visible irradiation. It should be noted that sunlight shows 60% of visible photons in comparison with a mere 4.5% of UV photons. So far, just very few works have been devoted to the study of these doped photocatalysts when incorporated into cementitious matrices [10].

The coating application of photocatalysts onto building materials is gaining a growing interest owing to several advantages [7]

(i) It allows applying active agents in pre-existing construction structures.

(ii) Active sites are located at the surface of the materials: this fact avoids the inclusion of the photocatalysts in the inner, inaccessible part of the matrices, thus yielding better performance of pollutants removal. Previous works have demonstrated how coatings of TiO_2 reach photocatalytic efficiencies of up to 60% whereas just a maximum of 45% was found for TiO_2 incorporated by

mass [11-12]. The fact that PCO requires the adsorption of the pollutant onto the active site of the photocatalytic additive should be kept in mind.

(iii) Coating application requires a lower consumption of photocatalytic additive than bulk addition: in a comparison between mortars coated with TiO_2 and mortars with TiO_2 in bulk, similar photocatalytic performances were found, although coating was loaded with 20 times less TiO_2 [11].

(iv) The presence of the additive on the surface of the materials can lead to changes in their hydrophilicity (photo-induced superhydrophilicity). As a consequence, materials exhibit self-cleaning performance: the reduction of the water contact angle (WCA) allows the water to easily remove the dirt (oily smog, dust, carbonaceous particles …) [13-15].

The easily washable surfaces would also contribute to the long run activity of the photocatalytic additives, since the final products of the PCO would be expected to be removed by the water sweep.

It has to be noticed, however, that some researchers warn about problems ascribed to the WCA reduction: the increased wettability of the surface of the building materials could give rise to an increase in water absorption that would negatively affect these materials [16]. Therefore, changes in the WCA are not desired to be accompanied by dramatic changes in the water transport phenomena of the treated materials.

Assuming the interest of these active coatings, different factors related to the characteristics of the substrate have a strong influence on the performance of these modified materials: roughness, pore size distribution, chemical and mineralogical composition, which can affect the adhesion of the coating [17-18]. The last point is strongly related to the loss of efficiency of these active coatings after weathering or abrasion phenomena [19]. Substrates with high porosity and roughness have shown better retention of particles of the photocatalysts, thus enhancing the resistance of the materials to different degradation mechanisms [20]. Literature shows successful coating applications onto limestone, bricks, cement and lime mortars [21-22]. Two different strategies have been put forward [23]: dispersion of titania nano-particles in organic carriers with adjuvant water repellent compounds (based, among others, on poly-alkyl-siloxanes, acrylic polymers …) [24-27] or water dispersions of the active nano-particles [28-31]. High color variations and compatibility problems have been mentioned as main concerns referring to the first approach. The second approach, with the use of aqueous dispersions, appears to be much more environmentally friendly and low-cost. However, nano-particles tend to combine forming aggregates, agglomerates, and flocs, some of them with strong bonds, reducing the active sites of the photocatalysts. Conventional

methods of stirring cannot guarantee a proper dispersion of the nano-particles [32]. In this line, very limited research has been devoted to the optimization of the aqueous sprayable suspensions in order to achieve better performance of the coatings. Particularly it is very important to reach a good dispersion of the nano-particles of the photocatalysts with the aim of: 1) increasing the number of active sites and 2) enhancing the electron-hole separation in order to prevent their eventual recombination that suppresses the photocatalytic activity [33-34].

The combination of the photocatalysts with superplasticizers, which act as dispersing agents, can thus lead to more efficient coatings and it is precisely the main focus of the current work. Four superplasticizers (SPs), compatible with cement matrices, were chosen as the subject matter of this study: three different polycarboxylate ethers derivatives were synthesized and comparatively studied versus a naphthalene-based superplasticizer. Their interactions in aqueous dispersions with nano-structured titania and Fe- and V-doped titania were studied. Active coatings were applied onto cement and air lime mortars. The effect of the different superplasticizers was assessed by studying the photocatalytic efficiency in NOx removal under different illumination sources (UV, solar and visible light). Studies on the water contact angle modifications due to the presence on the surface of the mortars of the photocatalysts were also carried out to estimate the potential self-cleaning ability of these coatings. The work also reports changes in the water absorption, capillarity and water vapour permeability of the treated mortars and their microstructural examination. Finally, artificial accelerated weathering was applied to the treated mortars to assess the long run performance of these coatings.

1.1. Background on superplasticizers

Superplasticizers are common admixtures used in cementitious matrices in order to improve workability of the plastic mixtures avoiding the excess of mixing water [35]. When added to cement-based systems, these molecules exhibit a dispersing action between cement particles due their electrostatic repulsion and/or steric hindrance effects [36,37] preventing them from agglomeration. The last generation of superplasticizers belongs to the polycarboxylate ethers family which are based on a main backbone with carboxylic groups with side ethylene oxide unit chains. Consequently, at the alkaline pH of the cement media, the carboxylic groups appear deprotonated and negatively charged [38]. By means of these negative charges, polymeric molecules are adsorbed onto the positively charged surfaces of the cement particles. The dispersion effect takes place because of the steric effect induced by the polyethylene lateral chains as the predominant effect [39], and the electrostatic repulsion forces, as a minor contribution [40]. Previous works have studied the influence of the superplasticizer molecular

architecture on the properties of the cement mixtures [41,42] and in other binding systems [37]. These works have reported that the parameters with strong influence on the performance of the superplasticizers are the size of the side chains, the number of the carboxylic groups of the main backbone (as determined by their anionic charge density) as well as the presence of different substituting groups, with either hydrophobic or hydrophilic characteristics.

Polynaphtalenesulfonate (PNS) belongs to the high-range water reducers in the field of cement materials. The molecular structure is characterized by a hydrophobic moiety (naphthalene) and a hydrophilic part (sulfonic groups). Electrostatic repulsive forces have been put forward as the main responsible for the plasticizing effect of PNS, whereas steric hindrance was seen to play a minor role. Strong negative values of the electrical charge of the cement particles were measured when PNS was adsorbed [43] and a monolayer flat adsorption has been suggested as the spatial interaction way [44].

In the present work, we will discuss the suitability of these superplasticizer molecules, which are highly compatible with cement-based systems, as dispersing agents of nano-structured photocatalytic additives, so that their PCO activity may be enhanced, with the final goal of optimizing coatings to be applied onto cement and air lime mortars conferring them depolluting and self-cleaning properties.

2. Materials and Methods

2.1. Materials

As photocatalysts, nano-particles of bare TiO_2 (Aeroxide P25, Evonik) and two different doped TiO_2, Fe- TiO_2 and V- TiO_2 synthesized by flame spray pyrolysis, FSP [9], were used. The two doped additives were supplied by Centro Tecnológico L´Urederra, Spain: Fe-TiO_2 was obtained by a solution of Fe^{3+} ion as precursor, whereas V-TiO_2 was obtained from a V_2O_5-TiO_2 mixture. According to the data provided by the supplier, further confirmed by X-ray photoelectron Spectroscopy (XPS), Ti^{4+} was substituted in the lattice by Fe^{3+} whereas titania doped with vanadium exhibited the superficial formation of heterostructures including vanadyl centers, TiO_2-VO_x.

Mineralogical and chemical compositions of these additives were also evaluated by X-ray fluorescence (XRF) and X-ray diffraction (XRD). Results showed that crystalline compounds were anatase and rutile (polymorphic forms of titania). Particle size of the crystallites was determined according to the Scherrer equation from the XRD results, yielding values of 21, 16 and 15 nm, respectively, for bare TiO_2, Fe-TiO_2 and V- TiO_2. In addition, specific surface area of the samples was assessed by N_2 adsorption isotherms at 77 K using an ASAP2020 (Micromeritics, USA) instrument and calculated using the

multipoint BET method. Values were 50, 101 and 113 m^2 g^{-1}, for bare TiO_2, Fe- TiO_2 and V- TiO_2, respectively.

The light absorbance of the photocatalysts was examined using a UV-2100 Shimadzu instrument. The UV–vis diffuse reflectance spectra were recorded in the wavelength range 300–800 nm. The doped additives showed increased absorption within the visible region, evidencing that these compounds increased their sensitivity towards visible illumination as compared with bare TiO_2. Further details on the characterization of these nano-particles can be found elsewhere [45].

Four different superplasticizers were used in order to optimize the coatings, three polycarboxylate-based polymers (previously synthesized according to procedures described elsewhere [42,46,47]) and a commercial PNS:

1) 52IPEG 5.8 is based on the copolymerization via free radical from acrylic acid and isoprenyl ω-hydroxy polyethylene glycol macromonomers [46]. Number of ethylene oxide units in the chain is 52 and acrylic acid and isoprenyl oxy poly(ethylene glycol) ratio is 5.8.
2) 23APEG contains α-allyl-ω-methoxy poly(ethylene glycol) macromonomers containing 23 ethylene oxide units and an equimolar amount of maleic anhydride [41]
3) 45PC6 is composed of methacrylic acid and the macromonomer ω-methoxy poly(ethylene glycol) methacrylate ester with 45 ethylene oxide units at a molar ratio of 6:1 [47].
4) A commercial PNS superplasticizer was also used (Melcret® 500F, BASF Construction Polymers, Trostberg/Germany) [48,49].

The study of the molecular properties of the superplasticizers was addressed in previous works [41,46-49]: their structures appear depicted in Fig. 1 and their main properties are summarized in Table 1.

The active coatings were applied onto the surface of hardened mortars obtained from two different binders: Portland Cement (PC) (type CEM II32.5 N, Portland) and dry slaked lime (class CL 90-S according to European standard [50], CALINSA, Spain). A siliceous aggregate was also used, which mineralogical composition and grading has been reported elsewhere [51].

2.2. Methods

2.2.1. Study of the diluted water dispersions of the photocatalytic additives

A Zetasizer Nano ZS apparatus (Malvern Instruments, Worcestershire, United Kingdom) was used to measure the particle size distribution of the suspensions of the photocatalytic additives (0.005%) and their aqueous dispersions with superplasticizers (0.01%). Measurements were repeated 3 times per sample and the average value was calculated. Before measuring, impurities were removed using a 0.2 μm filter (VWR, Darmstadt, Germany). In order to know the photocatalytic additive isoelectric points and zeta potential of the samples, measurements of the electrophoretic mobility of these samples were also done.

2.2.2. Obtaining of mortars

PC and air lime samples were selected as substrates owing to the wide areas of application of these kinds of mortars for building purposes. These mortars were prepared with a binder:aggregate ratio of 1:3 by weight. They were blended for 10 min at low speed in a mixer. Mixing water was then added and mixed for 90 s at low speed. The amounts of mixing water were 13% and 20% by weight of binder, for PC and air lime mortars, respectively. Afterwards, mortars were moulded in 40 mm of diameter x 36 mm of height cylindrical casts and de-moulded 24 h later (7 days later in the case of air lime samples). PC moulds were cured at 20°C and 95 % RH and air lime mortars were cured at 20 °C and 60% RH. PC mortars were cured for 28 days whereas air lime mortars were cured for 91 days to ensure a large extent of the carbonation. Cylindrical pieces (40 mm diameter and 10 mm of height) were sliced by using a Struers cutting-polishing machine to be used as supporting mortars for the coatings.

Pore size distributions of the substrates were obtained by mercury intrusion porosimetry (MIP) (Micromeritics-AutoPoreIV-9500; pressure 0.0015 to 207 MPa).

2.2.3. Preparation, study and application of coatings

Dispersions for coatings were prepared by dispersing the photocatalytic additive (1 wt. %) in water together with the superplasticizer (1 wt.% with respect to the photocatalysts) and were homogenised by mechanically stirring for 20 min. The concentration of the photocatalysts was chosen to guarantee the photocatalytic efficiency of the mortars without visible changes in colour or gloss [23].

An electroacoustic-based analyser (ZetaProbe, Colloidal Dynamics) was used to measure the zeta potential of the dispersions.

Adsorption tests of the SPs onto photocatalytic additives were also carried out. In a typical experiment 50 mL of the suspensions were centrifuged for 2 hours at 8000 rpm in a wobbler Heraeus Biofuge Stratos. The supernatant was taken and introduced in a

TOC-L Shimadzu Total Organic Carbon analyser. Total organic carbon (TOC) was determined by combustion at 680º C (NDIR detector). The adsorbed amount of superplasticizer was calculated between the difference of TOC content of polymer reference sample and the TOC content of the supernatant.

These suspensions were also examined in an energy filter transmission electron microscope (EFTEM, Libra 120 Zeiss GmbH). Images were obtained by using the software iTEM 5.1 (Olympus Soft Imaging Solutions GmbH).

The as-prepared coatings were applied onto discs of the hardened mortars as follows: discs were placed onto a flat area and coated with the previous dispersions using a spray gun for retouching Sagola 474 applying it for 6 s. Reproducible conditions were ensured to obtain similar coatings. Samples were weighed before and after the coating treatment. An average value of 28.5 mg of active dispersion was determined, so that the average percentage of photocatalytic additive with respect to the binder weight was 0.005%. Samples were dried by exposure to laboratory air (20ºC and 60% RH) for 48 hours. Blank discs were also obtained with untreated samples. As control groups, three samples of each material were covered with photocatalytic additive aqueous suspensions without SPs. A total of 15 coatings were thus obtained: 4 SPs and a control group (SP-free) combined with three different photocatalysts (bare TiO_2, Fe-TiO_2 and V-TiO_2). These coatings were respectively applied onto PC and air lime mortars.

2.2.4. Photocatalytic studies

Photocatalytic activity was studied in a flow-through experiment that has been adapted from an ISO standard method [53]. Experimental conditions were 50 ± 10% RH and 25 ± 2ºC. The cylindrical photoreactor (height 12 cm; diameter 14 cm) was fed by a 500 ppb NO stream. Concentrations of NO and NO_2 were determined by a chemiluminescence detector (Environnement AC32M) at a 0.78 L·min-1 flow. Experiments were carried out for discs of the samples prepared as above explained (height 1 cm; diameter 4 cm). The total exposed area of the discs was 25.14 cm^2. Irradiation was delivered by two different lamps: Osram Ultravitalux 300W, for UV illumination, and Philips SON-T PIA Plus 250W, for solar and visible irradiation, with intensities of 43.4 W m^{-2} and 36.7 W m^{-2}. A Traceable ultraviolet light meter Control Company (UV-A sensor 320-390 nm) and a Photo-Radiometer HD2302.0 Delta Ohm (visible sensor LP-471 RAD 400-1050 nm) were used in order to measure the intensities. In order to achieve strict visible radiation a colored glass filter (FGL420, Thorlabs) was used for solar radiation which cuts off completely wavelengths shorter than 410 nm. The UV-A light intensity has been selected as a mean value of these wavelengths irradiance for Southern Europe (clear sky day,

noon, summer time) [54]. The lamp used for solar light was calculated to provide around 10% of the intensity of the irradiation from 400-1050 nm determined for outdoor exposure in a sunny summer day (considering the solar constant as 1366 ± 2 W m^{-2} and the angle of incidence and the number of sunny hours, 342 W m^{-2} would be the average global power density at the top of the atmosphere. Just 70% reach the ground, so that an average value of 240 W m^{-2} can be estimated as the total solar irradiance (from which visible spectrum accounts for ca. 38-41% of the total irradiation).

NO_x stream flowed over the sample in the dark for 10 min in order to stabilize NO concentration. After that the photoreactor was irradiated for 30 minutes. NO concentration decreases until its minimum value. Then, the light was switched off for 10 minutes and NO concentration recovers its initial value. Error analysis of the experimental results obtained by this method, as expressed in terms of relative standard deviation, was calculated under reproducibility conditions to be 3.3% from replicate analysis of at least three identical samples.

2.2.5. Study of the properties of the mortars: water contact angle, time of water absorption, water absorption, capillary water absorption and water vapour permeability. Microstructural examination

The application of coatings is expected to modify some of the properties of the mortars, since the nano-structured photocatalysts would render hydrophilic the surface of the treated mortars. A video-based optical contact angle measuring instrument (OCA 15EC Dataphysics) was used to determine the static water contact angle (WCA) and time for water absorption (i.e. time for the water drop disappearance after its deposition, water drop lifetime, as a significant parameter for very porous substrates) [23]. WCA was determined using 3μL droplets and two consecutive measurements were performed for each sample in order to achieve reliable data.

To study the evolution of WCA under different types of radiation, samples were irradiated for 180 min under: (i) UV light; (ii) solar light; (iii) and visible light, using the illumination sources and conditions above described (section 2.2.4).

The study of other changes in the substrates as a consequence of the coating application was also performed by measurements of the water sorption including total water absorption (immersion), capillary water absorption and water vapour permeability. Hardened mortars were pre-treated for 30 days in a desiccator at 20ºC. After the coating application, treated mortars were allowed to dry at 20ºC and 60% RH for 2 days and then the tests were carried out.

These values are useful to establish the compatibility of the coatings with the specific substrates: a coating should not significantly increase the rate of water absorption and should not hinder the exchange of water vapour [23]. Water absorption of the mortars was determined by immersing the samples into distilled water. Sample weights were measured at 0 hours (before immersing) and 1 hour after the immersion. Water absorption capability was calculated by the difference of weight in percentage.

Capillary water absorption and water vapour permeability were determined following the rules described, respectively, in the standard procedures [55, 56].

Scanning Electron Microscopy combined with energy-dispersive X-ray microanalysis (SEM-EDS, FEI Instrument, Quanta 3D FEG, with INCA IE 350 Penta FET X-3 EDS, Oxford Instruments) was used for microstructural examination and elemental mapping of the treated mortars.

2.2.6. Durability

The assessment of the durability of the treatment applied to the samples was carried out after accelerated climatic ageing. Samples were placed in a climatic chamber (CCI FCH-XENOLAB 1500) with adjustable conditions of temperature (T), relative humidity (RH), UV light and rain cycles. Table 2 shows the characteristics of the set cycle, in accordance with previous works [57]. Mortars were subjected to a total of 7 cycles. Among the selected variables, rain washout and UV degradation are expected to be the main deleterious factors affecting the integrity of the coating. After the accelerated weathering, photocatalytic activity tests were run again to evaluate the loss of efficiency.

Samples subjected to accelerated weathering were also examined by SEM-EDS (see section 2.2.5 for details).

3. Results

3.1. Basic study on the water dispersions of the nano-structured additives

The surface charge of either the bare titania or the doped-titania nano-particles can be modified, as a function of the pH of the system. The dispersion of the nano-particles in water causes the formation of hydroxyl groups according to Eq. 1 [58]:

$$Ti^{IV} + H_2O \rightarrow Ti^{IV}{-}OH + H^+ \quad (1)$$

An acidic medium can lead to the positive protonation of the surface (Eq. 2)

$$Ti^{IV}{-}OH + H^+ \rightarrow Ti^{IV}{-}\ OH^+ \quad (2)$$

whereas deprotonation and subsequent negative charge of the surface takes place in an alkaline medium (Eq. 3):

$$Ti^{IV}-OH \rightarrow Ti^{IV}-O^{-} + H^{+} \quad (3)$$

Zeta potential measurements provide information about the charge of the surface of the particles (Fig. 2a). The three photocatalytic additives were characterized by studying their isoelectric points (IEP's), which were found to be 7.8; 7.3 and 6.1 for bare TiO_2, Fe-TiO_2 and V-TiO_2, respectively. In line with data reported in the literature, the presence of foreign cations (either Fe^{3+}, or V^{4+} as vanadyl centers) in the doped additives caused a reduction in the IEP value [59,60].

It can be observed (Fig. 2a) that at high pH, above 11, the three additives yielded strong negative values of zeta potential (below -30 mV), so that in these conditions the intense electrostatic repulsions between nano-particles would reduce their trend to agglomerate. The study of the behaviour of the photocatalytic additives in that high pH medium is crucial since coatings are to be applied onto highly alkaline cement or air lime mortars. Particle size distribution of the additives was studied in a Synthetic Cement Pore Solution (SCPS) dispersion medium [61]. Experimental results (depicted in Fig. 2b) show the tendency of the three nano-structured additives to form agglomerates in the SCPS in spite of the negative zeta potential of the nano-particles at the pH of the SCPS. In order to explain these results, two factors have to be considered: (i) even at very alkaline pH values well above the IEP, zeta potential could be not negative enough as to stabilize all the individual nano-particles. As a matter of fact, titania agglomerations have been reported in systems with alkaline pH [62,63]. (ii) The presence of a large concentration of Ca^{2+} cations caused a sharp increase of the ionic strength, simultaneously reducing the thickness of the double layer which, in turn, resulted in a decrease of the repulsive forces thus leading to an agglomeration [58,64-65].

In order to improve the photocatalytic activity an appropriate dispersion of the nano-particles appears to be imperative [66]. Thus, the incorporation of superplasticizers, as dispersing agents, gains interest.

Before studying the basis of the interaction of the different superplasticizers with the photocatalytic additives, preliminary experiments of Ca^{2+} adsorption onto the photocatalysts were carried out in alkaline aqueous dispersions [67]. The aim of these experiments was to determine the necessary amount of Ca^{2+} ions to change the surface charge of the nano-particles from negative to neutral charge. These Ca^{2+}-adsorbed nano-particles should become an appropriate substrate for the interaction with the negatively charged molecules of the superplasticizers, as explained before [67]. Fig. 2c depicts the curves obtained for the three types of nano-particles upon titration with

increasing Ca^{2+} amounts. These experiments yielded saturation values of 2.9, 5.1 and 5.8 mg Ca^{2+} per mg of TiO_2, Fe-TiO_2 and V-TiO_2, respectively.

Profiles of the zeta potential evolution for the three respective nano-particles suspensions upon the progressive addition of the four different superplasticizers (Fig. 3 a-c) were obtained at pH 12.5 in the presence of the experimentally optimized concentrations of Ca^{2+}. The incorporation of superplasticizers resulted in a decrease of the zeta potential in all instances. This finding evidences the adsorption of the superplasticizers molecules onto the previously created Ca^{2+} ions layer surrounding the photocatalysts nano-particles. It was found that, in both bare TiO_2 and Fe-TiO_2, the PNS yields the most negative zeta potential values, which can be accounted for having in mind the high anionic charge of this admixture as well as its flat adsorption favoured by its molecular structure [48,49].

The effect of the four assayed SPs on the particle size distributions of the three photocatalysts suspensions was also studied (Fig. 3 d-f). A general positive effect, in terms of preventing particles from agglomeration, was observed for all the combinations of SPs and photocatalysts, with the clear exception of PNS with V-TiO_2. Control samples (SP-free) presented the main population peak around a particle diameter of 700 nm. Particle size distributions showed a shift towards lower sizes upon the addition of superplasticizer admixtures. In many samples, the main population peak of the agglomerates was ca. 100 nm of diameter (see, for example, curves for bare TiO_2). Some of the SPs admixtures caused an acute reduction of the resulting agglomerate size: for instance, 23APEG added to bare TiO_2 yielded a main population of particles with 45 nm of diameter. On the other hand, and in spite of the strong negative zeta potential values, when PNS was added to V-TiO_2 suspensions, its presence led to the formation of larger flocs.

It can be seen that there was not a clear relationship between the shift of the zeta potential towards negative values and the efficiency in preventing nano-particles from agglomeration. The different performance of the superplasticizers can be ascribed to several factors, such as the molecular architecture of the SPs (the density and size of the side chains and the anionic charge density) and the particle size and chemical composition of the surface of the nano-particles. In the tested medium, 52IPEG showed good dispersing ability, which can be related to the length of its side chains that caused a strong steric hindrance, thus reducing the particle agglomeration. A neat dispersing effectiveness was also observed for both 45PC6 and 23APEG, in spite of the absence of a systematic trend. Efficiency can be explained considering the length of the side chains as well as their density. For example, whereas 45PC6 shows longer side chains than

23APEG (which should favour the steric hindrance), it shows lower density of side chains than 23APEG (which would result in a lower steric effect). A counteraction of both parameters takes place, explaining the similar efficiency of the two admixtures.

Regarding the zeta potential, 45PC6 usually caused a smaller reduction, when compared with 23APEG, in spite of the higher anionic charge density of the former. Its long side chains plausibly lead to a perpendicular adsorption offering a strongly negatively charged polymer layer on top of which the Ca^{2+} ions are adsorbed, partially compensating the negative charge [68]. In addition, the length of the side chains provokes a displacement of the shear plane to a longer distance from the nanoparticle what also contributes to a less negative value of the zeta potential [69].

PNS showed a good dispersing ability of the nano-particles for both bare TiO_2 and Fe-TiO_2 that can be mainly ascribed to electrostatic repulsions, as evidenced by the largest negative values of the zeta potential measured. However, an opposite behaviour was found for the case of V-TiO_2. The different structure of the surface of the V-TiO_2 has to be considered: the surface of the V-TiO_2, as proven by XPS examination, was rather composed of heterostructures comprising TiO_2 and VOx (vanadyl) centers (Fig. 4 shows the XPS survey spectra (a) and peaks related to V2p 3/2 and V2p 1/2 (b), which appeared at 515.8 and 523.7 eV, respectively, mainly related to the presence of vanadyl centers with V^{4+} [70-73]. A complete characterization of these additives appears in [74]: details of survey spectra and V region are shown here for clarity purposes); this additive also showed the highest specific surface area. These facts justified the highest consumption of Ca^{2+} ions, as discussed above, found necessary to compensate its charge. This secondary positively charged Ca^{2+} layer facilitated the simultaneous interaction of different nuclei of V-TiO_2 nano-particles with the strongly negatively charged molecule of PNS, inducing the formation of large flocs (with a mean particle size diameter as large as 1800 nm) as depicted in Fig. 3f.

3.2. Dispersing effectiveness of the superplasticizers in the coatings

After the preliminary study showing the effectiveness of the superplasticizers in avoiding the nano-particles agglomeration, different water dispersions of the photocatalysts (1 wt. %) with SPs were obtained. In this section the characteristics of these aqueous dispersions are discussed. These dispersions, as will be reported below in section 3.3, were later applied as coatings onto the surface of hardened mortars.

Zeta potential values versus increasing amounts of SPs were monitored, and the curves appear depicted in Fig. 5. Even at the acidic pH of the dispersions (see pH values in Table 3) a decrease of the surface charge of the nano-particles was observed caused by the SPs adsorption. In these results, the higher the anionic charge density of the

polymer, the stronger the zeta potential drop. Conversely to our previous results discussed in Fig. 3 (a-c), in these dispersions the absence of Ca^{2+} as potential determining ions hindered the charge compensation of the adsorbed polymer allowing a linear relationship for the zeta potential profiles. The shift of the shear plane by the side chains of the polymer showed here a very limited influence on the zeta potential.

As collected in Table 3, the higher the anionic charge density of the SPs, the higher the amount adsorbed. Thus, PNS, which has the highest anionic charge density, is just the only SP that caused a surface charge inversion of the three tested nano-particles, giving rise to the strongest zeta potential reduction.

Zeta potential of some of the tested dispersions fell within the instability region (aprox. between +25 and -25 mV). However, in line with the results discussed above in section 3.1., neither the adsorption onto the nano-particles nor the negative values of the zeta potential justified the observed dispersing effectiveness. TEM micrographs of the dispersions clarified the effectiveness of the SPs (Fig. 6). Bare TiO_2, Fe-TiO_2 and V-TiO_2 aqueous dispersions evidenced the formation of dense agglomerates of particles (average size around 845 nm for bare TiO_2, 445 nm for Fe-TiO_2 and 378 nm for V-TiO_2). Micrographs showed that the presence of the 52IPEG and 23APEG SPs prevented the nano-particles from agglomeration (size of the agglomerates between 180 nm and 290 nm), being 52IPEG the most effective superplasticizer according to the lower size of the nano-particles flocs formed. PNS exhibited an opposite behaviour, with a clear tendency to generate agglomeration of nano-particles. Finally, 45PC6 presented a dual behaviour, reducing the population of small flocs on one side, but, on the other side, also increasing the size of some large agglomerations (see In Fig. 7 complementary TEM micrographs of these additive suspensions, with some flocs).

These values were further confirmed by particle size distribution measurements (Fig. 8). These PSD curves must be cautiously discussed, as the media have a large concentration of nano-particles, presenting high values of polydispersity index. Bearing that in mind, some useful comparisons can be made. In all media, 52IPEG and 23APEG caused a reduction in the particle size, with a shift of the distributions towards lower particle size diameters. Conversely, PNS yielded the largest agglomerations, in good agreement with the TEM observations. The formation of some flocs in the case of samples with 45PC6 was also observed in TEM micrographs, although PSD curve of the sample with V-TiO_2 did not evidence the formation of the observed large flocs due to the aforementioned problems with the experimental technique.

In order to overcome this limitation, laser diffraction measurements of the particle size distribution were carried out for 45PC6 dispersions, confirming the TEM examination with respect to the agglomeration of the nano-particles (Fig. 9).

In spite of the strong negative values of the zeta potential, PNS caused an opposite effect, very clearly in V-TiO_2 suspensions, with the formation of very large flocs (with 10 micrometres of diameter), in line with the effect reported in Fig. 3f. From a mechanistic point of view, the structure of the PNS and its flat adsorption as discussed above (section 3.1) explains this behaviour [48]. At the same time, polycarboxylate-based superplasticizers -in which steric hindrance was the main action mechanism-, yielded the best dispersing action.

In addition, the effect of non-adsorbed SPs molecules should be also considered. For example, although 52IPEG showed the lowest adsorption onto the nano-particles of the photocatalysts (Table 3), it was the most effective in preventing these particles from flocculation. The concentration of "free" superplasticizer molecules in the interstitial solution contributes to an increased steric hindrance between the particles hampering their agglomeration [43,75-76].

3.3 Study of the photocatalytic activity of the mortars with coatings

After proving the effectiveness of the SPs (especially the polycarboxylated polymers) in dispersing the photocatalysts, the different sprayable water dispersions with the SPs and one control group (SP-free) were applied as coatings onto hardened mortars, as described in section 2.2.3. NO abatement percentages of these mortars are depicted in Fig. 10. High NO removal rates were obtained: percentages generally above 30% and even 40% of NO degradation under UV light (Fig. 10a). In the tested coatings NO abatements were comparable irrespective of the supporting material. The smaller photonic efficiency of the solar and visible light resulted in lower percentages of NO removal under these illumination sources.

A positive effect of the superplasticizers based on polycarboxylate chains was observed. For example, under UV light, NO abatement was increased by an average value of 15%. In some cases, this value was very high, as in the case of 52IPEG with TiO_2, with a 26% of NO abatement increase with respect to the coating applied without superplasticizer Under solar irradiation also the use of these superplasticizers resulted in a sharp increase of the NO removal rates (76% of average increase), particularly in coatings applied onto air lime mortars and very significant for coatings with Fe-TiO_2 (Fig. 10b).

The NO abatements of these coatings under strict visible irradiation were also clearly enhanced by the presence of polycarboxylate-based superplasticizers, as can be observed in Fig. 10c.

This improvement can be ascribed to the changes in the particle size distribution of the photocatalysts. As discussed in the previous section, the polycarboxylate-based

superplasticizers, mainly 52IPEG and 23APEG, reduced the agglomeration of the nano-particles of the photocatalytic additive, which resulted in more exposed active sites. In addition, the separation between active sites also gave rise to a decrease of the electron-hole recombination rates that also contributed to the enhancement of the photocatalytic activity [33-34].

Values of NO abatement with PNS were, however, lower than control group, in agreement with the agglomeration of the photocatalysts determined for this superplasticizer in coating dispersions, as discussed in section 3.2 (fig. 6 and Fig. 8).

Results of the 45PC6 superplasticizer were positive in terms of photocatalytic activity, which was generally increased. In spite of the formation of some large-sized flocs, the reduction of the size of the small agglomerates that was observed resulted in an enhancement of the NO removal.

The use of doped TiO_2 improved the efficiency of the photocatalytic oxidation under visible light, being Fe-TiO_2 generally more active than V-TiO_2. Under solar light, the UV light fraction of the irradiation source explains the still strong NO abatements of the bare TiO_2 coatings. Fe-TiO_2 also yielded large NO degradation percentages. An in-depth discussion on the effect of different doped additives under several illumination sources is beyond the scope of the present paper; a thorough study can be found elsewhere [9,70,74,77]. The main conclusion is that the combination of the nano-particles aqueous dispersions with polycarboxylate-based SPs enhanced the activity of the coatings under all the tested irradiation spectra.

Comparative analysis of the results of NO abatement from the current work with previous literature was also carried out. The activity of the coatings was always studied under UV light. In coatings of TiO_2 with acrylic binder, maximum NO removal percentages of 50% were reported, although the coatings showed a very high percentage of TiO_2 (15%), whereas coatings with a load of TiO_2 of 5% applied to different substrates provided NO removal efficiencies lower than 40% [78]. Coatings based on cement-water with 5% of TiO_2 have been reported to remove 26.9% of NO [79]. Values around 51-53% of NO removal were reported for coatings in which TiO_2 was incorporated either in a siliconate, water-based concrete sealer, or, directly, dispersed in water, although percentages of TiO_2 (14.3% and 11.8%) were much higher than those used in the current work [80]. Coatings with a similar TiO_2 load (1.15%) to that used in the current work yielded ca. 33% of NO removal [80].

In the current research work, coatings with just 1% of TiO_2 yielded NO removal percentages under UV light close to or even above 50%. The lower consumption of photocatalytic additive (and also the low superplasticizer concentration), while

significantly reducing the atmospheric NO, involves a clear economic improvement also minimizing environmental concerns related to the production and release of TiO_2.

3.4 Effect of the coatings on the mortars: water contact angle, time of water absorption, water absorption, capillarity and water vapour permeability. Microstructural examination

Water contact angle measurements were carried out to assess the hydrophilicity of the surface of the treated mortars and their wettability. As discussed in the Introduction, a high hydrophilicity could be related to the dirt-prevention ability of the treated mortar [81]. Measurements of the WCA were carried out under the three different irradiations: UV, solar and visible lights for 3 hours (Fig. 11). The most significant changes in the values of contact angle were achieved in the first 60 minutes of the experiments as it has been also reported by other authors [14,82]. Due to the roughness of the surface of the specimens, water contact angle did show attenuated changes in comparison with values reported for non-rough surfaces (like glass surfaces [83]) in which the presence of photocatalysts reduced the WCA to almost 0º.

Blank PC samples which were not coated with any photocatalytic additive, exhibited the highest contact angles in comparison with all the rest of PC samples, which shows that photocatalytic additive coatings increase hydrophilicity of the treated mortars.

Moreover, differences between contact angles measured for samples coated with either bare titania or Fe- or V-doped titania do appear at the initial stage of the experiment, t = 0 h. Thus, WCA values tend to be slightly greater for samples coated with just bare titania than for the samples coated with the other two doped photocatalytic additives. This fact can be explained considering the different hydrophilicity of the photocatalytic nano-particles as inferred from XPS analysis (Fig. 12). Deconvolution of the O 1s region resulted in three different peaks, being the second one (531.5 eV) related to the Ti-OH groups. Height and width of this peak informs about the hydrophilicity of the sample. Experimental results showed that the doping of the titania lattice with either Fe or V caused an enlargement and widening of this second peak and it can be concluded that Fe-TiO_2 and V-TiO_2 showed higher hydrophilicity than bare TiO_2, in line with data reported in a previous work [84].

The incorporation of any of the assayed superplasticizers did not bring in any noticeable changes in the WCA behaviour.

It can also be seen that UV irradiation of coated samples caused a more pronounced decay in contact angle values than either solar or visible irradiations (Fig. 11). This fact is in good agreement with previous findings [85] in which UV irradiation makes surfaces to become highly hydrophilic due to structural changes of TiO_2. When TiO_2 surface is

subjected to UV light, oxygen vacancies are generated owing to the reaction between diffuse photogenerated holes and lattice oxygen of TiO_2. These oxygen vacancies are favourable sites for water adsorption which favours a higher hydrophilic surface [84].

For samples with high porosity and significant population of large pores (in this case air lime mortars), WCA cannot be measured since water drop was quickly absorbed by the porous material. Total porosity in PC mortars was determined to be 14.9% whereas a value of 33.3% was obtained for air lime mortars. Instead, the time for water absorption (i.e. time taken by the water drop to disappear) was used to gather information on the wettability of the surface [23]. Experimental values in Fig. 13 (results shown only for UV light) showed that lime samples always presented –as expected- much shorter values (ca. 100 ms) than PC samples due to their pore size distribution (the main population of pores being larger than 0.5 micrometres and another two more population of pores with diameter around 3.8 and 9 micrometres). The presence of photocatalysts shortened the time for water absorption in agreement with the increased hydrophilicity of the surfaces. The decay in times followed a parallel pattern under all three assayed illumination types and no substantial differences were observed upon incorporation of any of the superplasticizers.

To assess the real applicability of the tested coatings, water transport phenomena were evaluated. It should be kept in mind that these phenomena were not assessed under any specific light exposure. If coating induces an excessive value of water uptake of the mortar (either water absorption or capillary water absorption), the water movement inside the structure can damage it through efflorescence phenomena [31,86]. Experimental results are depicted in Table 4 after 1 h of water immersion. As it can be seen, lime samples exhibited higher values, logically due to their higher porosity and different pore size distribution than PC samples (see Fig. 14).

No significant deviations were found for any of the lime samples from the averaged 15.5% water absorption. Generally, the application of coatings with Fe-TiO_2 caused a reduction in the water uptake. PC samples presented lower water absorption values, around 2%, the highest departures being observed for TiO_2 + 45PC6 and V-TiO_2 + 23APEG. Apparently, there is no clear reason based on the structure of the SPs to justify these values in these two specific OPC samples, although it should be noticed that 45PC6 and 23APEG show the larger molecular weight of the polycarboxylated molecules. This factor could show an influence on the water retention capacity of these polymers and also on the coatings with these SPs.

Capillary water absorption was also monitored for the different samples (Fig. 15 a-b). The application of the coatings (either with SPs or without SPs) reduced the capillary water absorption coefficients; this is due to the deposition of nanoparticulated

photocatalysts that led to blockage of the external capillary pores responsible for the water absorption. The use of the most hydrophobic superplasticizer, PNS, gave rise to the sharpest reductions in the capillary water absorption, since this dispersing agent created a hydrophobic layer on the surface of the mortars that hindered the absorption of water by capillarity.

This finding was also confirmed by measurements of the water vapour permeability, in Fig. 15 c-d. The use of PNS rendered the mortars less permeable to the water vapour (as expressed by the increase in the water vapour diffusion resistance coefficient) [23]. Building materials need an acceptable vapour permeability level to allow water vapour transport between inside and outside of the building. In this way, water retention and condensation in the material are avoided as well as the transport of damaging ions [87,88]. Due to their higher porosity and different pore structure, air lime mortars presented higher permeability values than PC samples. Apart from the use of PNS, above discussed, it can be said that superplasticizers did not impact negatively on water vapour permeability in lime mortars: values of the water vapour diffusion resistance coefficients underwent slight increases with respect to discs of untreated mortars (0%). These increases can be well understood assuming the blockage on the surface of some pores responsible for the vapour transport phenomena owing to the spread of nanoparticle-based coatings. In comparison with the control group (dispersion of nano-particles without any SP), the use of polycarboxylates, particularly 52IPEG, improved the dispersion of the nano-particles with a lower reduction of the permeability. This fact can be observed specially in PC mortars: the use of polycarboxylate-based SPs in comparison with control samples (coating applied without SPs) yielded better values of the water vapour permeability.

SEM-EDS observations (top view and cross section) were made to study the microstructure of the coatings and the distribution of the photocatalysts. Air lime mortars with bare TiO_2 are discussed below as an example. Top view micrographs showed that the nanoparticles of the photocatalysts gave rise to a spongy microstructure (Fig. 16a). Outcroppings of calcite crystals (determined by EDS) were also observed scattered by the treated surface of the mortars (Fig. 16b and a detailed view of these calcite crystals in Fig. 16c). The use of SPs modified the textural aspect of the coating: whilst the coating of the aqueous dispersion (SP-free) showed a high degree of cracking (Fig. 16d), the dispersions with some of the SPs, mainly 52IPEG and 23APEG, yielded a reduced number of cracks in the coating layer, as can be observed in some SEM micrographs (Fig. 16e and Fig. 16f). This fact can be ascribed to the different thickness of the deposited layer due to the distinct fluidity of the dispersions.

The SP-free water dispersions, with lower fluidity, gave rise to a thicker layer (as proven by the analysis of the cross section, in Fig. 16 h-j), with a lower degree of percolation within the monolithic mortar, as evidenced by the Ti mapping of this section (Fig. 16i). This aqueous layer lost the excess of water by evaporation, causing a large number of drying shrinkage cracks, mud cracking (see Fig. 16g) [89]. The thickness of the layer (measured value of ca. 20 microns) is well above the critical cracking thickness. Quantitative Ti EDS calculation yielded 47.3% in this active coating, due to the accumulation of the photocatalyst and the low dispersing effectiveness of the dispersion agent.

However, the use of superplasticizers increased the fluidity of the dispersions, allowing the obtaining of thinner coating layers (see, as an example, the lower thickness of the layer in the coating with 52IPEG, Fig. 16, micrographs k, l and m, of ca. 3-4 microns). This fact improved the percolation of the active photocatalyst, as denoted in the Ti mapping of the cross section (Fig. 16 l), and it is advantageous for practical applications in order to keep photocatalytic activity after abrasion phenomena that can involve loss of the external active compound. The adherence to the support was better in this case (coating with 52IPEG). The use of plasticizers also caused a reduction of the shrinkage cracks, in agreement with the use of plasticizers reported in previous works [90]. Quantitative Ti calculation by EDS confirmed the better distribution of the Ti per surface area, with, for example, values of 20.5% for 52IPEG and 30.3% for 23APEG. This finding would contribute to explain the enhancement of the NO removal, reducing the recombination sites.

3.5 Durability studies

In order to evaluate the durability of the efficiency of the coatings, the treated mortars were subjected to accelerated ageing in a climatic chamber according to the cycles described in section 2. Afterwards, NO abatements tests under UV irradiation, as selected irradiation, were carried out for all aged samples (Fig. 17). The accelerated weathering process caused a reduction in the NO degradation ability of the treated mortars. Mainly the washout by rain water of the photocatalysts and, secondly, the degradation of the coatings caused by UV light, would explain this reduction. The weathering conditions simulated a total amount of accumulated rain water of 4032 mm. Considering that the average cumulative precipitation in the region of Navarra (north of Spain) is 820 mm per year, in line with calculations made previously by other researchers [7,23], this rainfall value would correspond to 5 years of degradation.

Control mortars (without SPs) showed an average 33.8% decrease of removal efficiencies for PC samples and 28.6% for air lime samples. For coatings with SPs, PC

mortars yielded a similar average decrease of 35.2% whereas air lime mortars only decreased the NO removal ability by 16.4%. This fact can be explained considering that an increase in porosity and roughness of the surface of the mortars enhances the retention of the photocatalytic nano-particles, in line with the findings of previous works [20]. Taking into account the higher porosity and larger pore size of the main pore population of air lime mortars (Fig. 14), photocatalysts were better retained in these mortars, withstanding the accelerated weathering. Irrespective of the supporting matrix, the superplasticizer that yielded the lowest loss of efficiency was PNS, because the hydrophobicity of its molecular structure helps to reduce the washout by rain water of the active nano-particles. Among the polycarboxylate-based superplasticizers, 52IPEG, with 24.6% of average reduction, was the most efficient in preserving the activity of the coatings. 23APEG and 45PC6 yielded higher losses of the NO removal efficiencies: 31.6% and 29.2%, respectively. A similar argument can be used to understand these differences: 52IPEG showed higher hydrophobicity (longer side chains) than 23APEG and 45PC6, so that coatings with this SP prevent active nano-particles from being washed off. In addition, the largest fluidity of the coatings with 52IPEG enhanced the percolation of the photocatalysts, as discussed previously, thus contributing to their lower removal by rain water.

In spite of the aggressive conditions of the accelerated weathering, coatings with superplasticizers based on polycarboxylate chains still showed relatively high NO removal values. In general, PC mortars showed values above 20% (reaching in some cases 30% or even 40%), whereas air lime mortars showed an even better performance with values generally above 30%. It should be noticed that these results were achieved for coatings with just 1 wt.% of active nano-particles.

SEM examination revealed that the climatic ageing caused a surface deterioration. In Fig. 17, micrographs of a PC mortar treated with TiO_2-23APEG allowed us to observe, after the accelerated ageing, the increase in pores and changes in the textural aspect, with the appearance of some disaggregated areas.

Quantitative analysis by EDS was also carried out. Replicates in different areas showed an initial 5.8% of elemental Ti, whereas after the weathering this percentage was lowered to 4.9%. In agreement with the NO removal after the ageing, coatings showed a good degree of resistance against climatic factors, as proven by the relatively low TiO_2 loss. This finding has positive environmental implications, since the dangerous release of nano-particles of these coatings has been low. The loss of efficiency of NO removal can be thus ascribed to the small washout of active material as well as to the poisoning of some active sites of the photocatalysts.

Few previous works dealt with the loss of NO removal efficiency after accelerated climatic ageing in coatings. Real weathering has been reported to decrease NO removal efficiency by 36% and even up to 78% after 4 months of exposure [91]. In outside weathering, samples with active coatings exposed 4 months and with a final washing with water evidenced very significant loss of efficiency, with decreases above 50-70% [80]. For coatings applied in concrete pavements, accelerated rotary abrasion tests yielded a 16.7% of decrease of the NO abatement efficiency [79]. In this last case, the coating was loaded with 5% of TiO_2, so that the loss of the photocatalyst due to the wearing was minimized. For a plaster with TiO_2 added in bulk, similar accelerated weathering cycles decreased the NO abatement by 45.5% [92]. The main conclusion is that the use of SPs to optimize coatings with photocatalytic agents provides systems with a significant resistance to weathering.

4. Conclusions

Water-dispersions coatings of different nano-particles of photocatalytic additives (titania and titania doped with iron and vanadium) have been prepared with diverse superplasticizers to optimize the NO removal efficiency.

The study of the aqueous dispersions showed that the use of polycarboxylate-based superplasticizers (52IPEG, 23APEG and 45PC6) prevented nano-particles from agglomeration. However, the use of a naphthalene sulfonate formaldehyde polycondensate, PNS, resulted in the formation of large agglomerates of nano-particles. The steric hindrance, provided by a large density and length of side chains, was the most effective repulsion mechanism and 52IPEG was the most efficient SP. In addition, the concentration of remaining “free” superplasticizer molecules in the interstitial solution contributed to an increased steric hindrance between the particles.

When the coatings were applied onto PC and air lime mortars, the polycarboxylate-based SPs improved the NO removal rates as compared with the SP-free coating: for example, an average increase of NO degradation by 15% under UV and by 76% under solar light was found. The higher photocatalytic efficiency was related to the reduction in the agglomeration of the photocatalysts, with more exposed active sites and a decrease of the electron-hole recombination rates.

The presence of the photocatalyts caused a reduction of the static water contact angle under UV, solar and visible light illumination, which is positive to the dirt-prevention ability of the mortars.

To assess the real applicability of these coatings, measurements of water absorption (by immersion), capillary water absorption and water vapour permeability showed that the

mortars were not altered in their performance upon the addition of the polycarboxylated-based coatings.

Microstructural examination, included the cross section analysis, showed that the use of SPs enhanced the distribution of the photocatalysts yielding thinner coating layers. The increased fluidity of the fresh coatings due to the presence of the SPs boosted the percolation of the active material within the mortars reducing the drying shrinkage cracks of the coating.

Durability of these coatings under accelerated weathering was good: NO removal efficiency reduction was moderate (35% for PC mortars and 16% for air lime mortars). Among the polycarboxylate-based superplasticizers, 52IPEG, with 24.6% of average reduction, was the most efficient in preserving the activity of the coatings. Measurements of SEM-EDS of Ti content showed a low washout of the TiO_2 nano-particles, supporting the long-run activity of these coatings.

Acknowledgments

This work was funded by MINECO, under grant MAT2015-70728-P. The research leading to these results has received funding from "la Caixa" Banking Foundation. M. Pérez-Nicolás thanks the Friends of the University of Navarra, Inc., for a pre-doctoral grant.

References

1. Y. S. H. Najjar, Gaseous pollutants formation and their harmful effects on health and environment, Innovative energy policies. 1 (2011) 1-9.

2. G.M. Masters, E. Wendell, Introduction to environmental engineering and science (3rd ed) Prentice Hall, Upper Saddle River, N.J, 2008.

3. J. S. Dalton, P. A. Janes, N. G. Jones, J. A. Nicholson, K. R. Hallam, G. C. Allen, Photocatalytic oxidation of NOx gases using TiO_2: a surface spectroscopic approach, Environ. Pollut. 120 (2002) 415-422.

4. M. Pérez-Nicolás, J. Balbuena, M. Cruz-Yusta, L. Sánchez, I. Navarro-Blasco, J.M. Fernández, J.I. Alvarez, Photocatalytic NOx abatement by calcium aluminate cements modified with TiO_2: Improved NO_2 conversion, Cem. Concr. Res. 70 (2015) 67-76.

5. A. Folli, C. Pade, T. B. Hansen, T. De Marco, D. E. Macphee, TiO_2 photocatalysis in cementitious systems: Insights into self-cleaning and depollution chemistry, Cem. Concr. Res. 42 (2012) 539-548.

6. S.S. Lucas, V.M. Ferreira, J.L. Barroso de Aguiar, Incorporation of titanium dioxide nanoparticles in mortars — Influence of microstructure in the hardened state properties and photocatalytic activity, Cem. Concr. Res. 43 (2013) 112-120.

7. A. Maury-Ramirez, K. Demeestere, N. De Belie, Photocatalytic activity of titanium dioxide nanoparticle coatings applied on autoclaved aerated concrete: effect of weathering on coating physical characteristics and gaseous toluene removal, J. Hazard. Mater. 211 (2012) 218-225.

8. L. Cassar, Photocatalysis of cementitious materials: clean buildings and clean air, Mrs Bulletin, 29 (2004) 328-331.

9. S. N. R. Inturi, T. Boningari, M. Suidan, P. G. Smirniotis, Visible-light-induced photodegradation of gas phase acetonitrile using aerosol-made transition metal (V, Cr, Fe, Co, Mn, Mo, Ni, Cu, Y, Ce, and Zr) doped TiO_2, Appl. Catal. B 144 (2014) 333-342.

10. J. D. Cohen, G. Sierra-Gallego, J. I. Tobón, Evaluation of photocatalytic properties of Portland cement blended with titanium oxynitride (TiO_2−xNy) nanoparticles, Coatings 5 (2005) 465-476.

11. P. Krishnan, M. H. Zhang, L. Yu, H. Feng, Photocatalytic degradation of particulate pollutants and self-cleaning performance of TiO_2 containing silicate coating and mortar, Constr. Build. Mater. 44 (2013) 309-316.

12. J. O. Carneiro, S. Azevedo, V. Teixeira, F. Fernandes, E. Freitas, H. M. R. D. Silva, J. Oliveira, Development of photocatalytic asphalt mixtures by the deposition and volumetric incorporation of TiO_2 nanoparticles, Constr. Build. Mater. 38 (2013) 594-601.

13. A. M. Vidaković, J. G. Ranogajec, S. L. Markov, E. S. Lončar, H. M. Hiršenberger, A. S Škapin, Synergistic effect of the consolidant and the photocatalytic coating on antifungal activity of porous mineral substrates, J. Cult. Herit. 24 (2017) 1–8.

14. C. Garlisi, G. Scandura, G. Palmisano, M. Chiesa, C. Y. Lai, Integrated nano and macroscale investigation of photoinduced hydrophilicity in TiO_2 thin films, Langmuir 32 (2016) 11813-11818.

15. M. Miyauchi, N. Kieda, S. Hishita, T. Mitsuhashi, A. Nakajima, T. Watanabe, K. Hashimoto, Reversible wettability control of TiO_2 surface by light irradiation, Surf. Sci. 511 (2002) 401-407.

16. E. Quagliarini, F. Bondioli, G. B. Goffredo, C. Cordoni, P. Munafò, Self-cleaning and de-polluting stone surfaces: TiO_2 nanoparticles for limestone, Constr. Build. Mater. 37 (2012) 51-57.

17. A. Calia, M. Lettieri, M. Masieri, Durability assessment of nanostructured TiO_2 coatings applied on limestones to enhance building surface with self-cleaning ability, Build. Environ. 110 (2016) 1-10.

18. C. Mendoza, A. Valle, M. Castellote, A. Bahamonde, M. Faraldos, TiO_2 and TiO_2–SiO_2 coated cement: Comparison of mechanic and photocatalytic properties, Appl. Catal. B 178 (2015) 155-164.

19. E. Boonen, A. Beeldens, I. Dirkx, V. Bams, Durability of Cementitious Photocatalytic Building Materials, Catal. Today Available online 18 October 2016.

20. A. M. Ramirez, K. Demeestere, N. De Belie, T. Mäntylä, E. Levänen, Titanium dioxide coated cementitious materials for air purifying purposes: Preparation, characterization and toluene removal potential, Build. Environ. 45 (2010) 832-838.

21. T. Martinez, A. Bertron, G. Escadeillas, E. Ringot, V. Simon, BTEX abatement by photocatalytic TiO_2-bearing coatings applied to cement mortars, Build. Environ. 71 (2014) 186-192.

22. Q. Li, Q. Liu, B. Peng, L. Chai, H. Liu, Self-cleaning performance of TiO_2-coating cement materials prepared based on solidification/stabilization of electrolytic manganese residue, Constr. Build. Mater. 106 (2016) 236-242.

23. E. Franzoni, A. Fregni, R. Gabrielli, G. Graziani, E. Sassoni, Compatibility of photocatalytic TiO_2-based finishing for renders in architectural restoration: A preliminary study, Build. Environ. 80 (2014) 125-135.

24. J. Radulovic, J. MacMullen, Z.Zhang, H. N. Dhakal, S. Hannant, L. Daniels, J. Elford, C. Herodotou, M. Totomis, N. Bennett, Biofouling resistance and practical constraints of titanium dioxide nanoparticulate silane/siloxane exterior facade treatments, Build. Environ. 68 (2013) 150-158.

25. P. N. Manoudis, I. Karapanagiotis, A. Tsakalof, I. Zuburtikudis, B. Kolinkeová, C. Panayiotou, Superhydrophobic films for the protection of outdoor cultural heritage assets, Appl. Phys. A-Mater. 97 (2009) 351-360.

26. Sh. K. Amin, N.M. Maarouf, S. S. Ali, Sustainable development of cultural Heritage via anti weathering nanoparticles material, Aust. J. Appl. Sci. 6 (2012) 227.

27. M. F. La Russa, S.A. Ruffolo, N. Rovella, C. M. Belfiore, A.M. Palermo, M. T. Guzzi, G. M. Crisci, Multifunctional TiO_2 coatings for Cultural Heritage, Prog. Org. Coat. 74 (2012) 186-191.

28. L. Graziani, E. Quagliarini, F. Bondioli, M. D'Orazio, Durability of self-cleaning TiO_2 coatings on fired clay brick façades: Effects of UV exposure and wet & dry cycles, Build. Environ. 71 (2014) 193-203.

29. A. Licciulli, A. Calia, M. Lettieri, D. Diso, M. Masieri, S. Franza, R. Amadelli, G. Casarano, Photocatalytic TiO_2 coatings on limestone, J. Sol-Gel Sci. Techn. 60 (2011) 437-444.

30. E. Quagliarini, F. Bondioli, G. B. Goffredo, C. Cordoni, P. Munafò, Self-cleaning and de-polluting stone surfaces: TiO_2 nanoparticles for limestone, Constr. Build. Mater. 37 (2012) 51-57.

31. E. Quagliarini, F. Bondioli, G. B. Goffredo, A. Licciulli, P. Munafò, Self-cleaning materials on architectural heritage: compatibility of photo-induced hydrophilicity of TiO_2 coatings on stone surfaces, J. Cult. Herit. 14 (2013) 1-7.

32. N. S. Allen, M. Edge, J. Verran, J. Stratton, J. Maltby, C. Bygott, Photocatalytic titania based surfaces: environmental benefits, Polym. Degrad. Stabil. 93 (2008) 1632-1646.

33. J. Li, S. Cai, Z. Xu, X. Chen, J. Chen, H. Jia, J. Chen, Solvothermal syntheses of Bi and Zn co-doped TiO_2 with enhanced electron-hole separation and efficient photodegradation of gaseous toluene under visible-light, J. Hazard. Mater. 325 (2017) 261-270.

34. F. Duo, Y. Wang, X. Mao, X. Zhang, Y. Wang, C. Fan, A $BiPO_4$/BiOCl heterojunction photocatalyst with enhanced electron-hole separation and excellent photocatalytic performance, Appl. Surf. Sci. 340 (2015) 35-42.

35. L. Crépy, J. Petit, E. Wirquin, P. Martin, N. Joly, Synthesis and evaluation of starch-based polymers as potential dispersants in cement pastes and self leveling compounds, Cem. Concr. Comp. 45 (2014) 29-38.

36. C. Z. Li, N. Q. Feng, R. J. Chen, Effects of polyethlene oxide chains on the performance of polycarboxylate-type water-reducers, Cem. Concr. Res. 35 (2005) 867-873.

37. I. Navarro-Blasco, M. Pérez-Nicolás, J.M. Fernández, A. Duran, R. Sirera, J.I. Alvarez, Assessment of the interaction of polycarboxylate superplasticizers in hydrated lime pastes modified with nanosilica or metakaolin as pozzolanic reactives, Constr. Build. Mater. 73 (2014) 1-12.

38. J. Plank, B. Yu, Preparation of hydrocalumite-based nanocomposites using polycarboxylate comb polymers possessing high grafting density as interlayer spacers, Appl. Clay Sci. 47 (2010) 378-383.

39. H. Uchikawa, S. Hanehara, D. Sawaki, The role of steric repulsive force in the dispersion of cement particles in fresh paste prepared with organic admixture, Cem. Concr. Res. 27 (1997) 37-50.

40. J. Plank, C. Hirsch, Impact of zeta potential of early cement hydration phases on superplasticizer adsorption, Cem. Concr. Res. 37 (2007) 537-542.

41. J. Plank, H. Li, M. Ilg, J. Pickelmann, W. Eisenreich, Y. Yao, Z. Wang, A microstructural analysis of isoprenol ether-based polycarboxylates and the impact of structural motifs on the dispersing effectiveness, Cem. Concr. Res. 84 (2016) 20-29.

42. A. Lange, T. Hirata, J. Plank, Influence of the HLB value of polycarboxylate superplasticizers on the flow behaviour of mortar and concrete, Cem. Concr. Res. 60 (2014) 45-50.

43. B.G. Kim, S. Jiang, C. Jolicoeur, P.C. Aïtcin, The adsorption behavior of PNS superplasticizer and its relation to fluidity of cement paste, Cem. Concr. Res. 30 (2000) 887-893.

44. Y. Zhang, X. Kong, Correlations of the dispersing capability of NSF and PCE types of superplasticizer and their impacts on cement hydration with the adsorption in fresh cement pastes, Cem. Concr. Res. 69 (2015) 1-9.

45. M. Pérez-Nicolás, I. Navarro-Blasco, J.M. Fernández, J.I. Alvarez, The Effect of TiO_2 Doped Photocatalytic Nano-Additives on the Hydration and Microstructure of Portland and High Alumina Cements, Nanomaterials 7 (2017) 329.

46. A. Lange, J. Plank, Optimization of comb-shaped polycarboxylate cement dispersants to achieve fast-flowing mortar and concrete, J. Appl. Polym. Sci. 132 (2015) 42529.

47. A. Lange, J. Plank, Contribution of non-adsorbing polymers to cement dispersion, Cem. Concr. Res. 79 (2016) 131-136.

48. J. Pickelmann, J. Plank, A mechanistic study explaining the synergistic viscosity increase obtained from polyethylene oxide (PEO) and β-naphthalene sulfonate (BNS) in shotcrete, Cem. Concr. Res. 42 (2012) 1409-1416.

49. L. Lei, J. Plank, Synthesis and properties of a vinyl ether-based polycarboxylate superplasticizer for concrete possessing clay tolerance, Ind. Eng. Chem. Res. 53 (2014) 1048-1055.

50. EN 459-1. Building lime. Part 1: definition, specification and conformity criteria, European Committee for Standardization, 2011.

51. I. Navarro-Blasco, A. Duran, R. Sirera, J.M. Fernández, J.I. Alvarez, Solidification/stabilization of toxic metals in calcium aluminate cement matrices, J. Hazard. Mater. 260 (2013) 89-103.

52. M. T. Rodríguez Laguna, R. Medrano, M. P. Plana, M. P.Tarazona, Polymer characterization by size-exclusion chromatography with multiple detection, J. Chromatogr. A 919 (2001) 13-19.

53. ISO 22197-1. Test Method for Air Purification Performance of Semiconducting Photocatalytic Materials. Part 1: Removal of Nitric Oxide, International Organization for Standardization, 2007.

54. M. D. P. Corrêa, Solar ultraviolet radiation: properties, characteristics and amounts observed in Brazil and South America, An. Bras. Dermatol. 90 (2015) 297-313.

55. EN 1015-18. Methods of test for mortars for mansonry. Part 18: Determination of water absorption coefficient due to capillary action of hardened mortar, European Committee for Standardization, 2000.

56. EN 1015-19. Methods of test for mortar for masonry. Part 19: Determination of water vapour permeability of hardened rendering and plastering mortars, European Committee for Standardization, 1999.

57. A. Izaguirre, J. Lanas, J.I. Álvarez, Ageing of lime mortars with admixtures: Durability and strength assessment, Cem. Concr. Res. 40 (2010) 1081-1095.

58. K. Suttiponparnit, J. Jiang, M. Sahu, S. Suvachittanont, T. Charinpanitkul, P. Biswas, Role of surface area, primary particle size, and crystal phase on titanium dioxide nanoparticle dispersion properties, Nanoscale Res. Lett. 6 (2010) 27.

59. B. Babić, J. Gulicovski, Z. Dohčević-Mitrović, D. Bučevac, M. Prekajski, J.Zagorac, B. Matović, Synthesis and characterization of Fe^{3+} doped titanium dioxide nanopowders, Ceram. Int. 38 (2012) 635-640.

60. M. Sahu, K. Suttiponparnit, S. Suvachittanont, T. Charinpanitkul, P. Biswas, Characterization of doped TiO_2 nanoparticle dispersions, Chem. Eng. Sci. 66 (2011) 3482-3490.

61. S. Baueregger, M. Perello, J. Plank, Role of PVOH and kaolin on colloidal stability of liquid and powder EVA and SB latexes in cement pore solution, Colloid. Surface. A 434 (2013) 145-153.

62. T. Hurnaus, J. Plank, Behavior of Titania Nanoparticles in Cross-linking Hydroxypropyl Guar Used in Hydraulic Fracturing Fluids For Oil Recovery, Energ. Fuel. 29 (2015) 3601-3608.

63. P.Wang, N. Qi, Y. Ao, J. Hou, C. Wang, J. Qian, Effect of UV irradiation on the aggregation of TiO2 in an aquatic environment: Influence of humic acid and pH, Environ. Pollut. 212 (2016) 178-187.

64. F. Loosli, P. L. Coustumer, S. Stoll, Effect of electrolyte valency, alginate concentration and pH on engineered TiO_2 nanoparticle stability in aqueous solution, Sci. Total Environ. 535 (2015) 28-34.

65. J. Jiang, G. Oberdörster, P. Biswas, Characterization of size, surface charge, and agglomeration state of nanoparticle dispersions for toxicological studies, J. Nanopart. Res. 11 (2009) 77-89.

66. F.Z. Haque, R. Nandanwar, P. Singh, Evaluating photodegradation properties of anatase and rutile TiO2 nanoparticles for organic compounds, Optik 128 (2017) 191-200.

67. A. Habbaba, J. Plank, Interaction between polycarboxylate superplasticizers and amorphous ground granulated blast furnace slag, J. Am. Ceram. Soc. 93 (2010) 2857-2863.

68. J. Plank, D. Vlad, A. Brandl, P. Chatziagorastou, Colloidal chemistry examination of the steric effect of polycarboxylate superplasticizers, Cem. Int. 3 (2005) 100-110.

69. J. Plank, B. Sachsenhauser, Impact of molecular structure on zeta potential and adsorbed conformation of α-allyl-ω-methoxypolyethylene glycol-maleic anhydride superplasticizers, J. Adv. Concr. Technol. 4 (2006) 233-239.

70. J. C.-S Wu, C. Chen, A visible-light response vanadium-doped titania nanocatalyst by sol–gel method, J. Photoch. Photobio. A, 163 (2004) 509-515.

71. J.Ph. Nogier, M. Delamar, Chapter 7.1 X-ray photoelectron spectroscopy of TiO_2/V_2O_5 catalysts, Catal. Today 20 (1994) 109-123.

72. T. Chen, H. Lin, B. Guan, X. Gong, K. Li, Z. Huang, Promoting the low temperature activity of Ti–V–O catalysts by premixed flame synthesis, Chem. Eng. J. 296 (2016) 45-55.

73. A. Vittadini, M. Casarin, M. Sambi, A. Selloni, First-Principles Studies of Vanadia−Titania Catalysts: Beyond the Monolayer, J. Phys. Chem. B 109 (2005) 21766-21771.

74. M. Pérez-Nicolás, I. Navarro-Blasco, J.M. Fernández, J.I. Alvarez, Atmospheric NOx removal: study of cement mortars with iron- and vanadium-doped TiO_2 as visible light-sensitive photocatalysts, Constr. Build. Mater. 149 (2017) 257-271.

75. C. Jolicoeur, J. Sharman, N. Otis, A. Lebel, M. A. Simard, M. Page, The influence of temperature on the rheological properties of superplasticized cement pastes. To be presented at the V.M. Malhotra (Ed.), Proceedings of the 5th CANMET/ACI International Conference on Superplasticizers and Other Chemical Admixtures in Concrete, ACI Symposium, Rome, 173 (1997) 379-406.

76. K. Yamada, S. Hanehara, K. Honma, Effects of Naphthalene Sulfonate-type and Polycarboxylate-type Superplasticizers on the Fluidity of Belite-rich Cement Concrete. Proceeding of Self-compacting Concrete Workshop, Kochi (1998) 201-210.

77. W. Y. Teoh, R. Amal, L. Mädler, S. E. Pratsinis, Flame sprayed visible light-active Fe-TiO_2 for photomineralisation of oxalic acid, Catal. Today 120 (2007) 203-213.

78. T. Martinez, A. Bertron, E. Ringot, G. Escadeillas, Degradation of NO using photocatalytic coatings applied to different substrates, Build. Environ. 46 (2011) 1808-1816.

79. M. M. Hassan, H. Dylla, L. N. Mohammad, T. Rupnow, Evaluation of the durability of titanium dioxide photocatalyst coating for concrete pavement, Constr. Build. Mater. 24 (2010) 1456-1461.

80. S. Shen, M. Burton, B. Jobson, L. Haselbach, Pervious concrete with titanium dioxide as a photocatalyst compound for a greener urban road environment, Constr. Build. Mater. 35 (2012) 874-883.

81. J. Y. Wang, H. J. Tsai, J.Y. Uan, M. S. Wong, S. K. Wu, Investigation of the photo-catalytic coating on AZ91 alloy, J. Alloy. Compd. 467 (2009) 257-260.

82. M.J. Twu, A.H. Chiou, C.C. Hu, C.Y. Hsu, C.G. Kuo, Properties of TiO_2 films deposited on flexible substrates using direct current magnetron sputtering and using high power impulse magnetron sputtering, Polym. Degrad. Stabil. 117 (2015) 1-7.

83. N. Sakai, R. Wang, A. Fujishima, T. Watanabe, K. Hashimoto, Effect of ultrasonic treatment on highly hydrophilic TiO_2 surfaces, Langmuir 14 (1998) 5918-5920.

84. M. Kang, The superhydrophilicity of Al–TiO_2 nanometer sized material synthesized using a solvothermal method, Mater. Lett. 59 (2005) 3122-3127.

85. M. Miyauchi, N. Kieda, S. Hishita, T. Mitsuhashi, A. Nakajima, T. Watanabe, K. Hashimoto, Reversible wettability control of TiO_2 surface by light irradiation, Surf. Sci. 511 (2002) 401-407.

86. M. Arandigoyen, J. P. Bernal, M. B. López, J. I. Alvarez, Lime-pastes with different kneading water: pore structure and capillary porosity, Appl. Surf. Sci. 252 (2005) 1449-1459.

87. A. Izaguirre, J. Lanas, J. I. Alvarez, Effect of water-repellent admixtures on the behaviour of aerial lime-based mortars, Cem. Concr. Res. 39 (2009) 1095-1104.

88. P. Maravelaki-Kalaitzaki, Hydraulic lime mortars with siloxane for waterproofing historic masonry, Cem. Concr. Res. 37 (2007) 283-290.

89. B.C. Bonekamp, Fundamentals of Inorganic Membrane Science and Technology, Chapter 6, Preparation of Asymmetric ceramic membrane supports by dip-coating, Ed. A.J. Burggraaf, ,L. Cot. . Elsevier Science (1996), pp178-183.

90. L.W. McKeen, Fluorinated Coatings and Finishes Handbook: The Definitive User's Guide. Front Matter, In Plastics Design Library, edited by Laurence W. McKeen, William Andrew Publishing, Norwich, NY, 2006, 302 p,

91. CM. Yu, Deactivation and regeneration of environmentally exposed titanium dioxide (TiO_2) based products. Environmental Protection Department, HKSAR 2003; Departmental Order Ref. No.: E183413.

92. B. Daniotti, S. Lupica Spagnolo, R. Galliano, The durability experimental evaluation of photocatalytic cement-based materials, Proceedings of the International Conference on Durability of Building Materials and Components, Porto, Portugal (2011) 1-8.

Table 1. Characteristics of the tested superplasticizers.

Superplasticizer	***Molar mass*** *(g/mol)*	***Polydispersity index*** *(Mw/Mn)*	***Specific anionic charge*** *(μeq/g)*
52IPEG	3.16×10^4	2.42	1,895
23APEG	4.60×10^4	2.76	1,695
45PC6	3.84×10^4	2.05	2,740
PNS	1.40×10^5	-	4,089

Table 2. Characteristics of the cycle of accelerated weathering

Cycle duration	*Step*	*Temperature (ºC)*	*Relative Humidity (%)*	*Rain*	*UV Light*	*Time (min)*
	1	35	30	No	Yes	160
	2	12	80	Yes	No	160
	3	20	50	No	No	160
	4	12	60	No	No	160
24 hours	5	35	30	No	Yes	160
	6	12	80	Yes	No	160
	7	35	30	No	Yes	160
	8	20	50	No	No	160
	9	12	60	No	No	160

Table 3. Values of pH of the final dispersions and adsorption percentages of the superplasticizers onto photocatalitic additives assayed

Superplasticizer	***TiO_2***		***Fe-TiO_2***		***V-TiO_2***	
	pH	*Adsorption (%)*	*pH*	*Adsorption (%)*	*pH*	*Adsorption (%)*
52IPEG	4.4	30.4	4.1	26.1	3.8	1.3
23APEG	4.4	58.1	3.9	75.7	3.8	51.5
45PC6	6.3	76.3	4.3	56.9	4.1	28.1
PNS	6.5	83.7	5.9	47.0	4.8	40.7

Table 4. Percentage of water absorption (1 h of immersion) of different PC and air lime mortars.

Composition		***Water absorption (%)***	
		PC	***Air lime***
Blank sample		2.20	15.58
	Control	1.98	15.52
	52IPEG	0.72	15.34
TiO_2	*23APEG*	1.20	16.25
	45PC6	5.80	15.63
	PNS	2.27	16.00
	Control	1.68	14.39
	52IPEG	1.28	14.89
Fe-TiO_2	*23APEG*	1.56	14.41
	45PC6	2.82	16.41
	PNS	2.58	15.05
	Control	1.82	16.34
	52IPEG	2.69	15.75
V-TiO_2	*23APEG*	5.63	16.67
	45PC6	1.81	15.14
	PNS	0.87	15.73

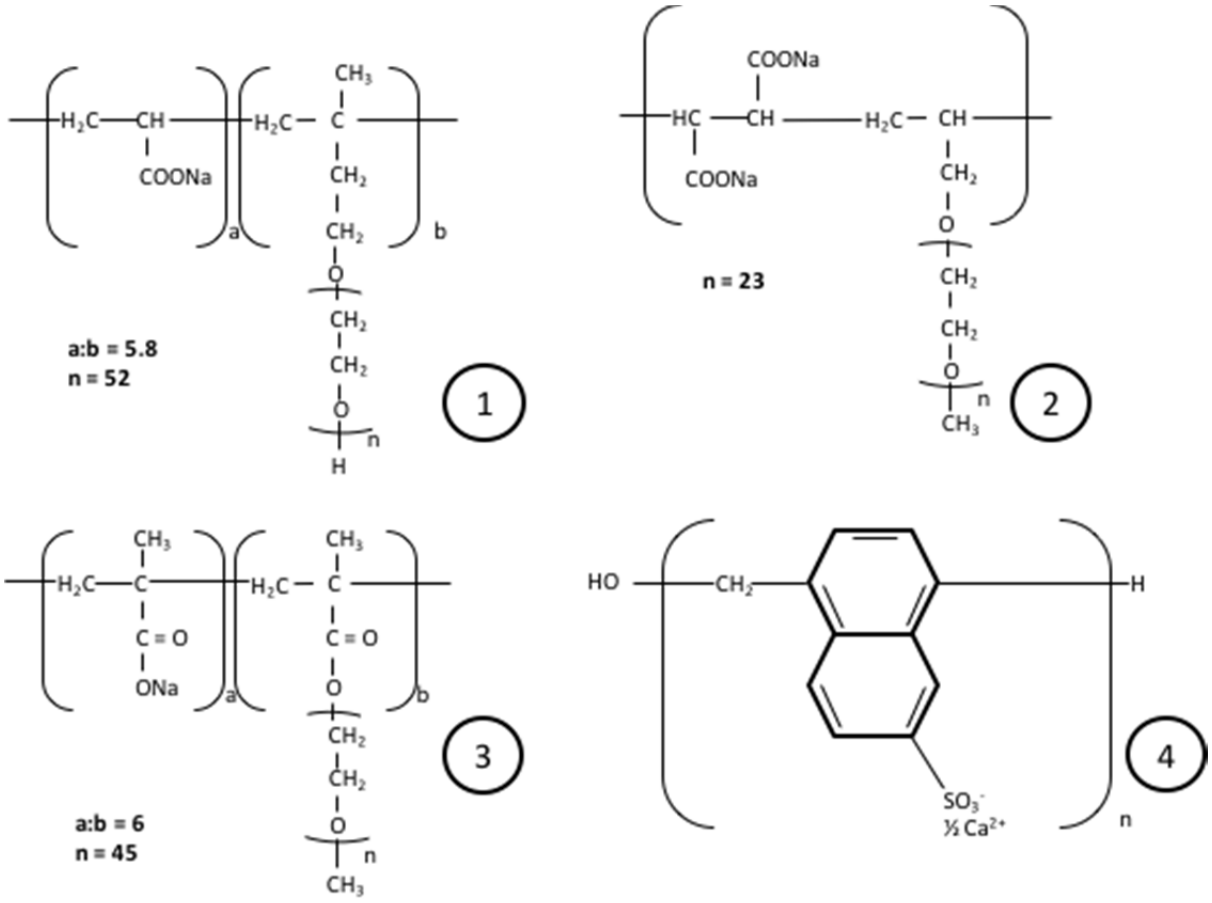

Figure 1. Molecular structures of the superplasticizers assayed: 1) 52IPEG, 2) 23APEG, 3) 45PC6, and 4) PNS.

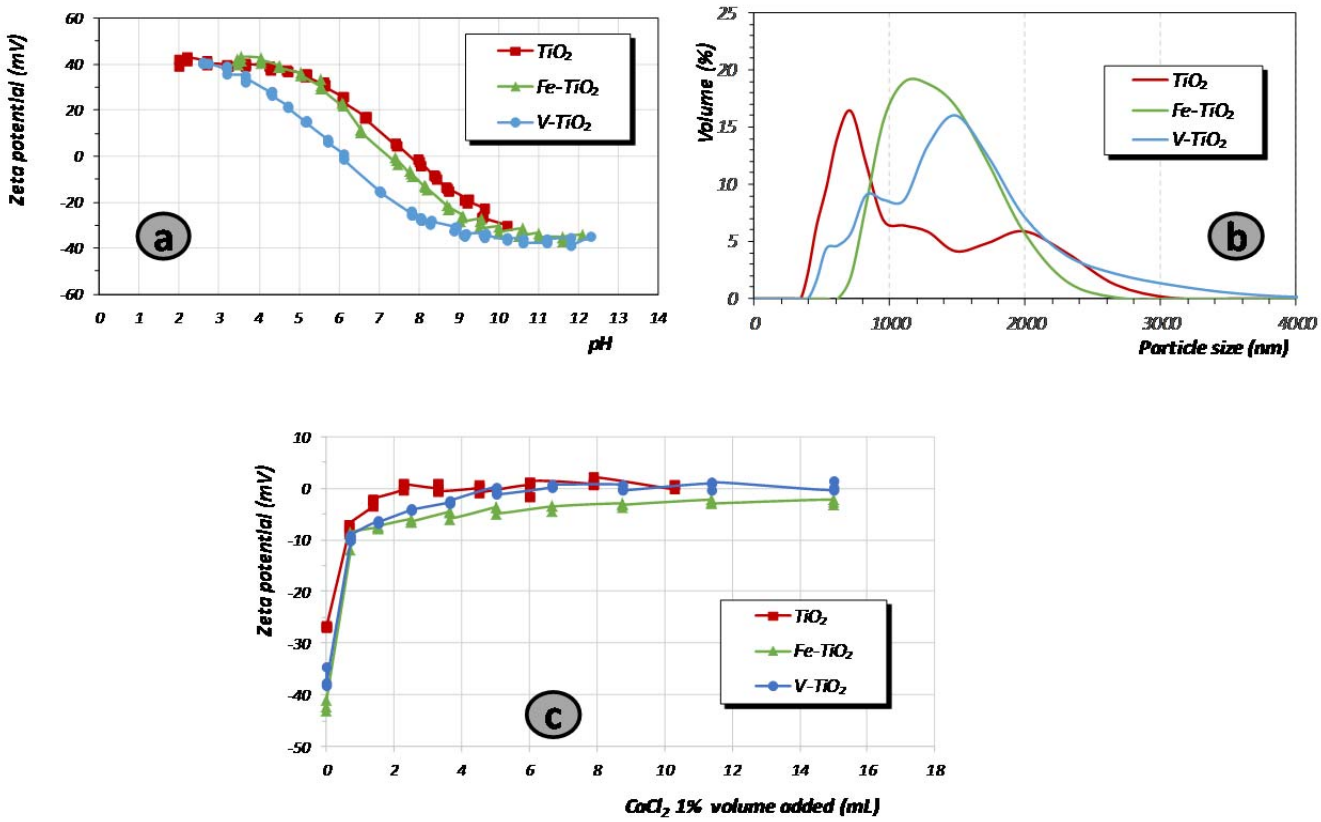

Figure 2. a) Zeta potential of the three photocatalytic additives assayed. **b)** Particle size distribution of the photocatalytic additives in SCPS. **c)** Zeta potential values of the photocatalytic additives suspensions titrated with a solution of calcium chloride 1%.

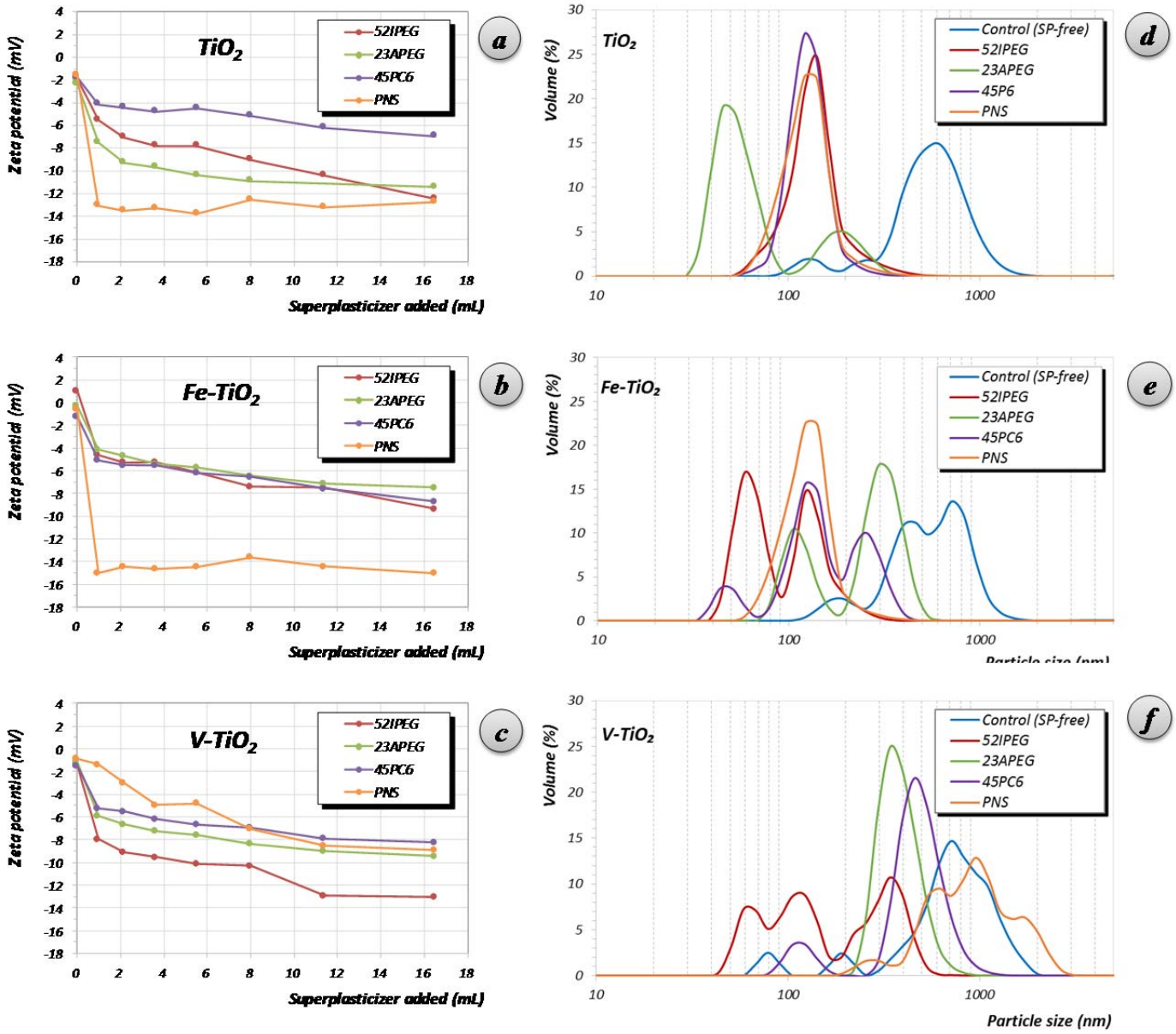

Figure 3. Data of the suspensions of the four superplasticizers assayed in optimized $CaCl_2$ concentrations at pH 12.5: Zeta potential values of a) bare TiO_2, b) Fe-TiO_2 and c) V-TiO_2 suspensions titrated with the four superplasticizers assayed. Particle size of d) bare TiO_2, e) Fe-TiO_2 and f) V-TiO_2 suspensions.

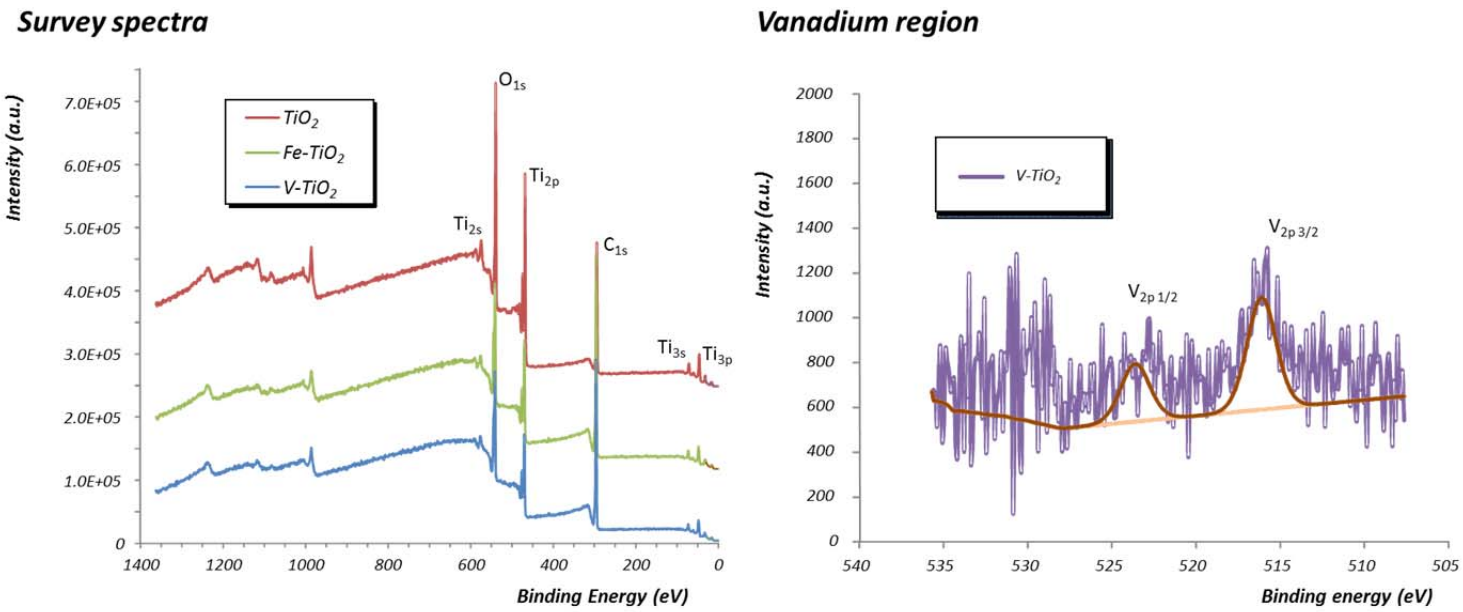

Figure 4. XPS results of the photocatalysts: survey spectra (left); V region for the V-TiO_2 sample (right).

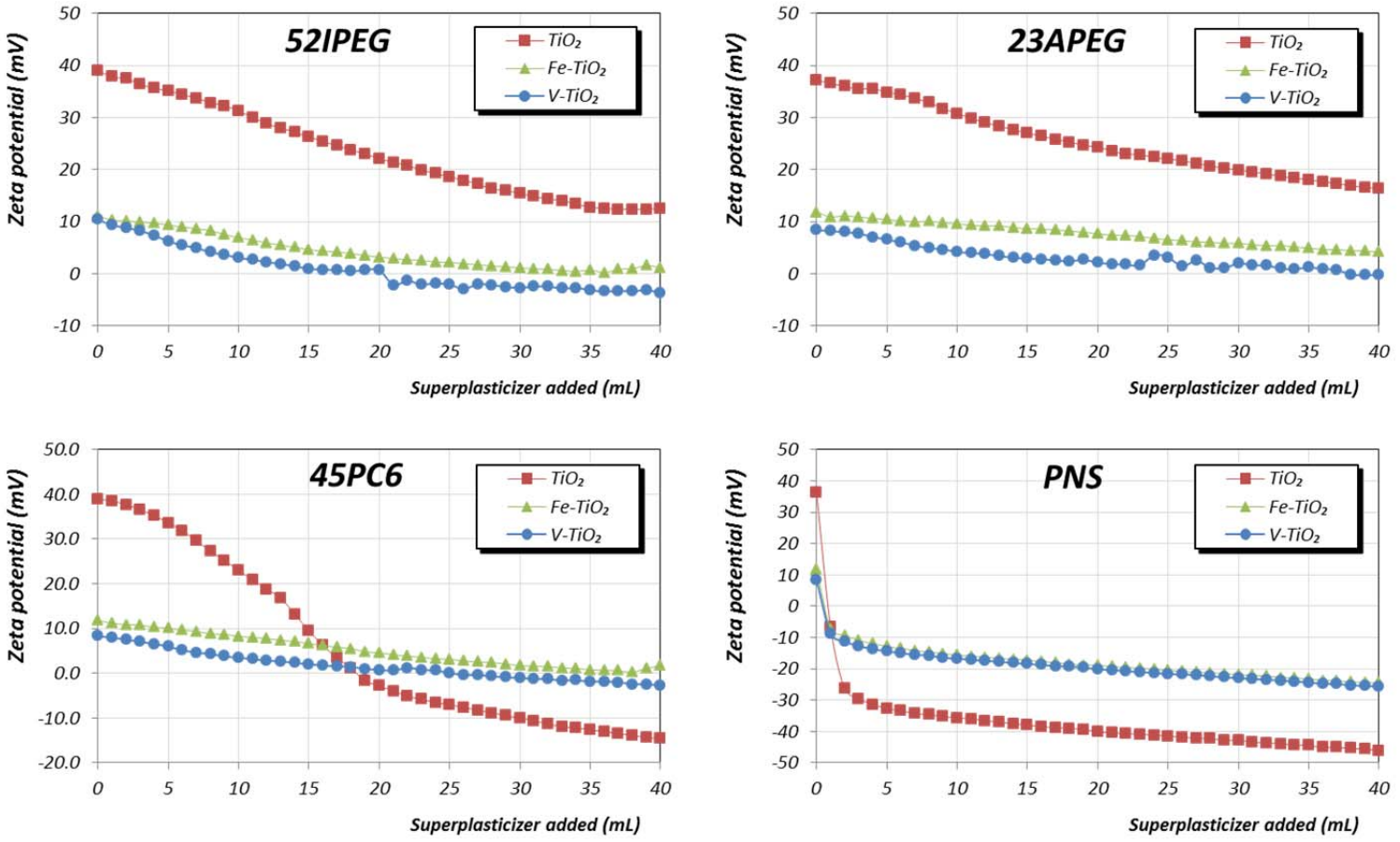

Figure 5. Zeta potential values of the concentrated water dispersions of photocatalytic additives titrated with the four superplasticizers assayed.

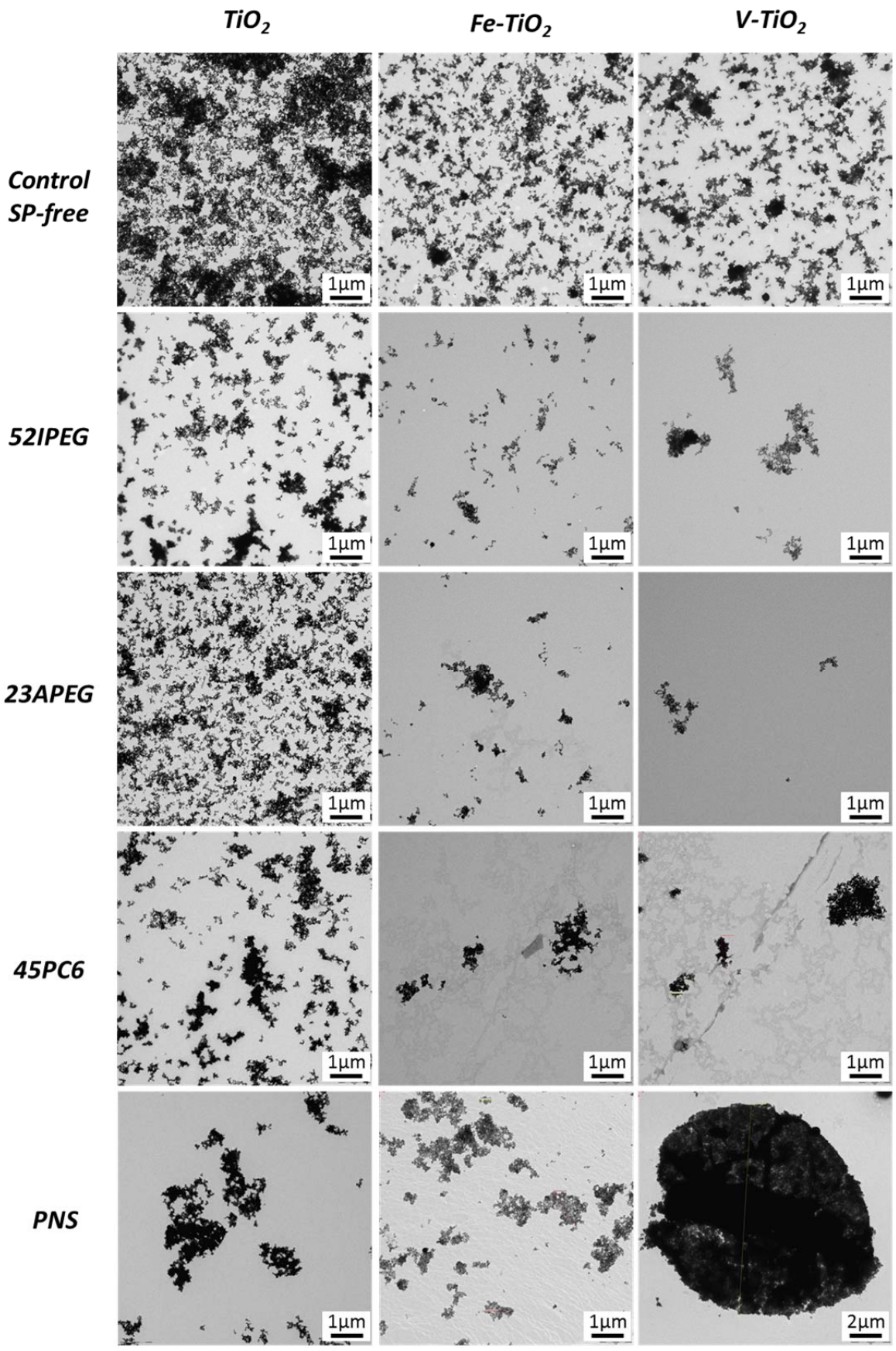

Figure 6. TEM micrographs of the photocatalytic additives dispersions.

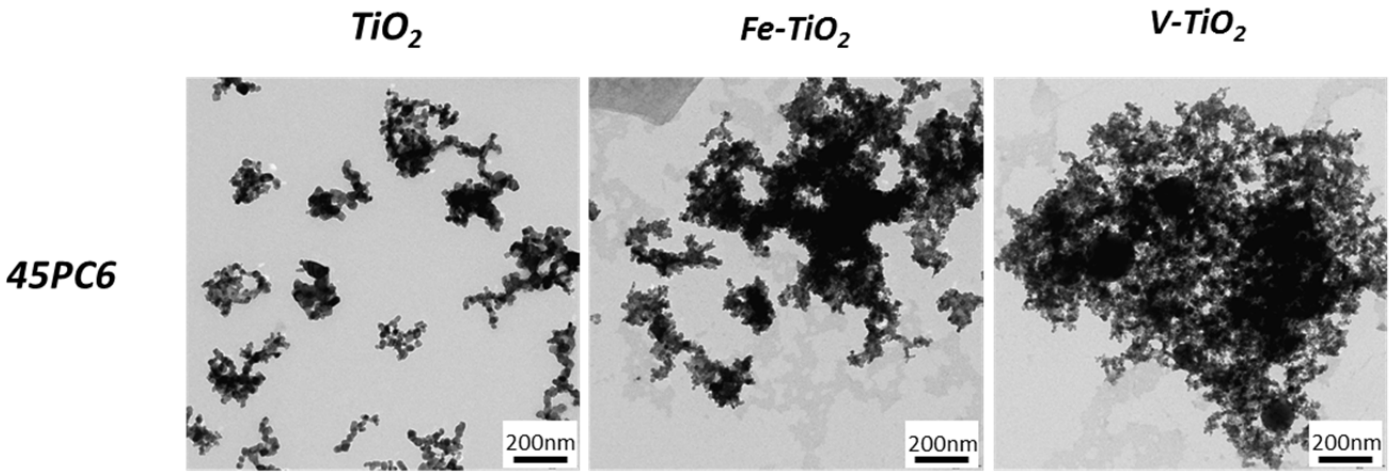

Figure 7. TEM micrographs of the photocatalytic additives suspensions with the superplasticizer 45PC6.

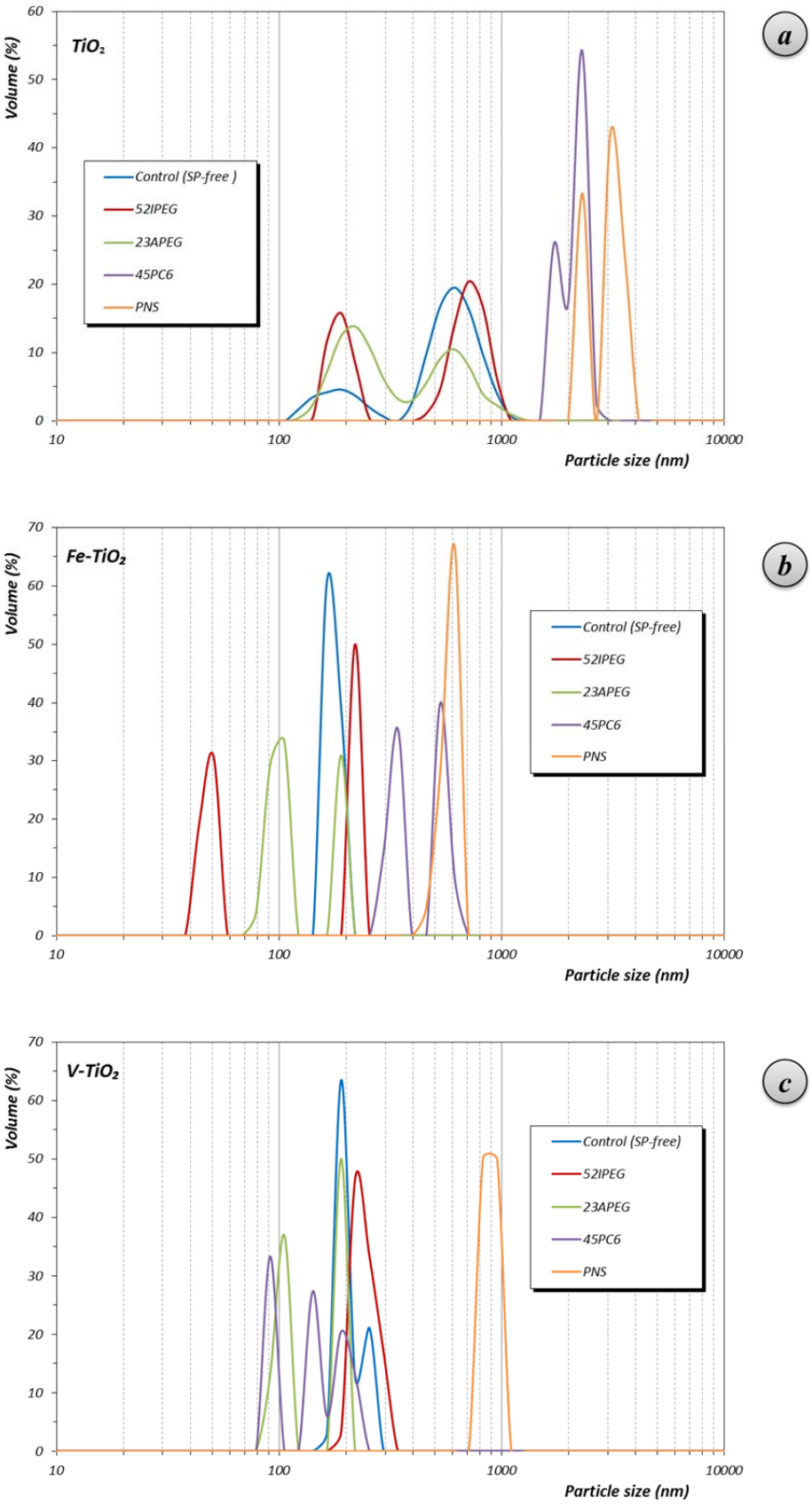

Figure 8. Effect of the SPs on the particle size distributions of a) bare TiO_2, b) Fe-TiO_2 and c) V-TiO_2 dispersions.

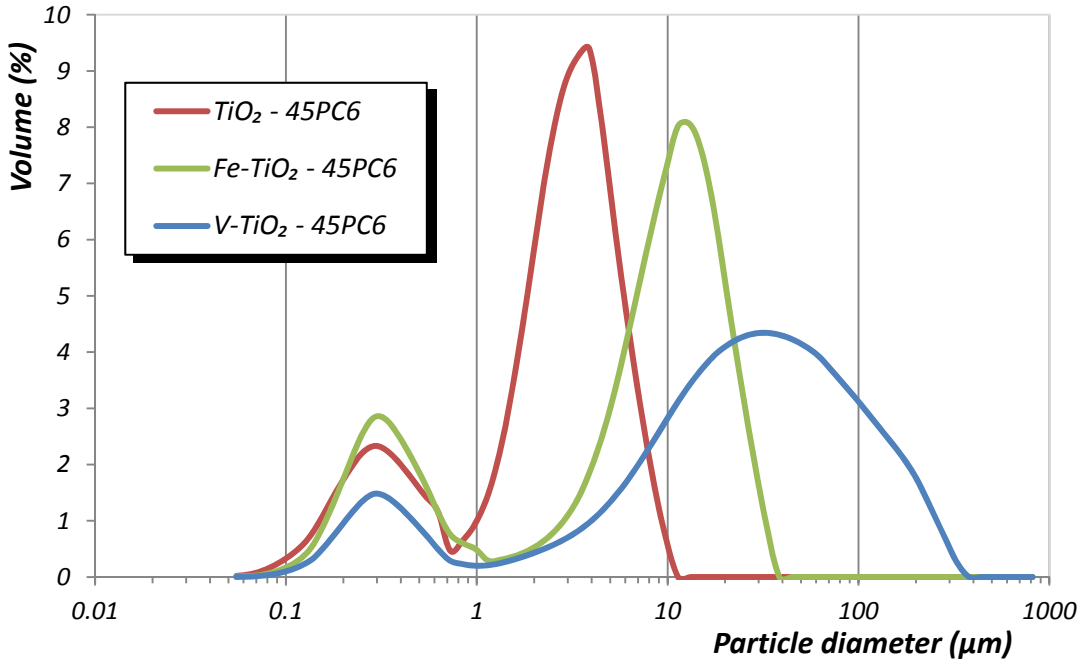

Figure 9. Particle size of photocatalytic additives dispersions with the superplasticizer 45PC6.

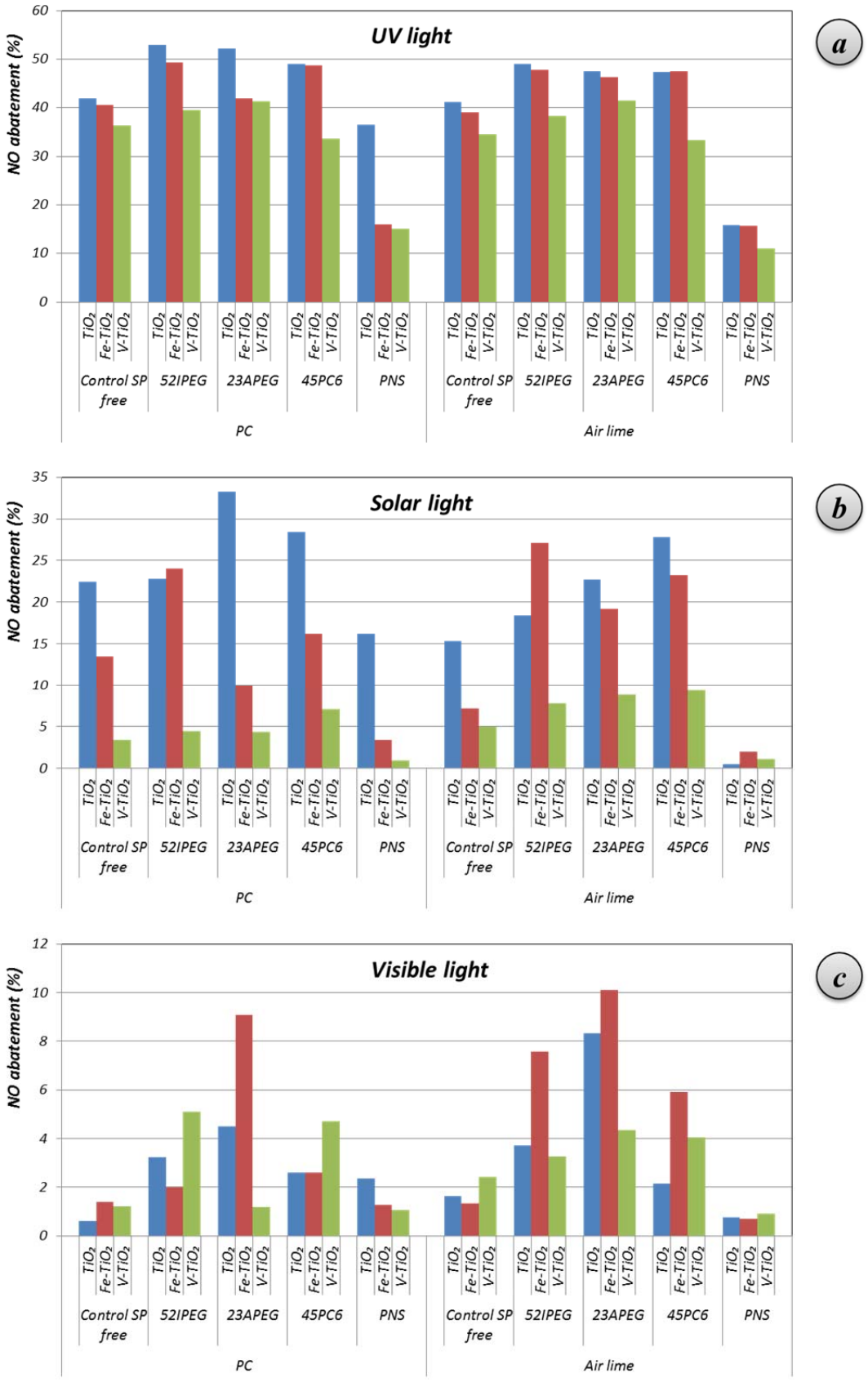

Figure 10. Percentages of NO abatement by different photocatalytic additives included in Portland cement and air lime mortars under: a) UV light; b) solar light; and, c) visible light.

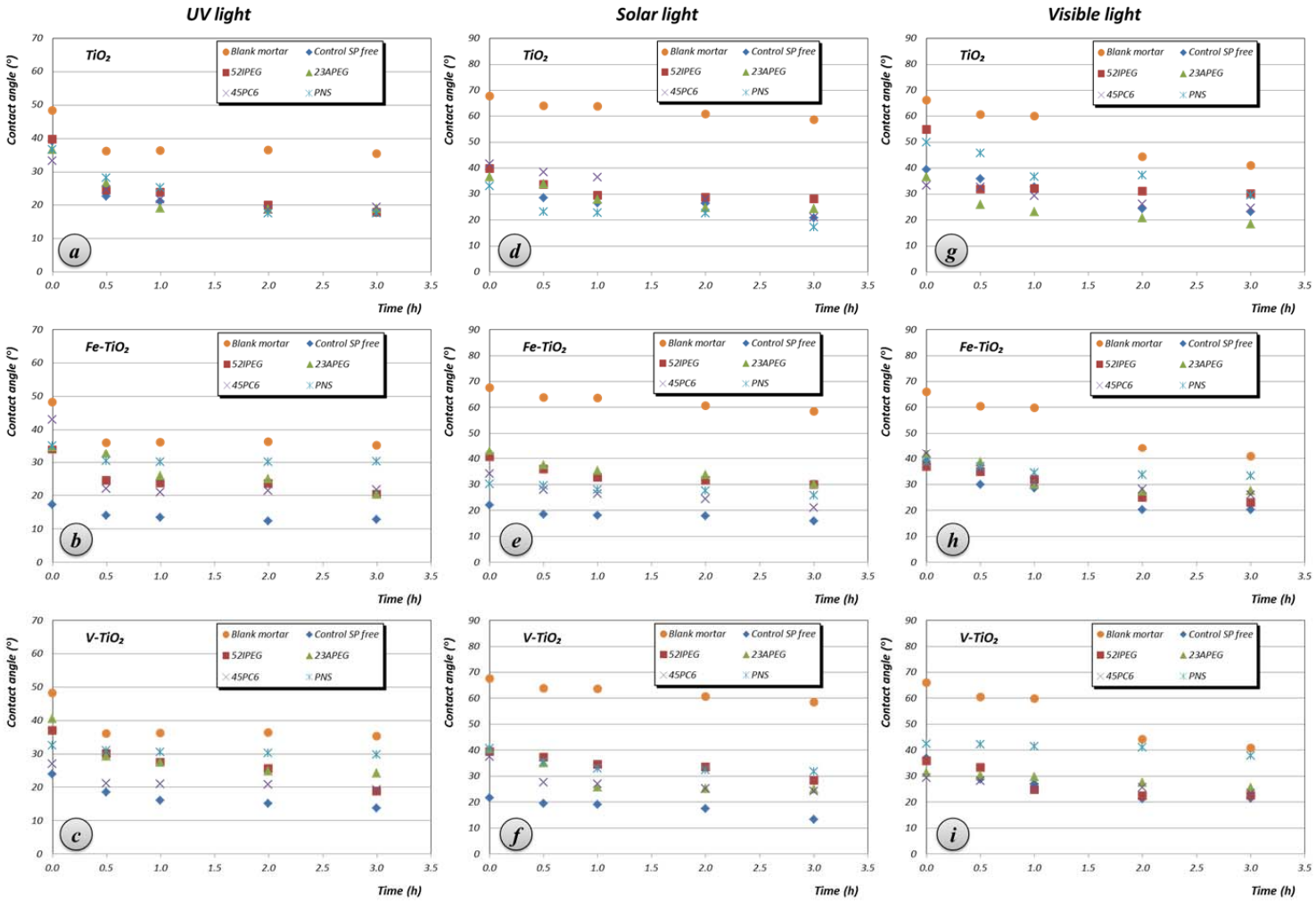

Figure 11. Water contact angle of PC mortars treated with different coatings vs. time of UV (a-c), solar (d-f) and visible (g-i) light exposition.

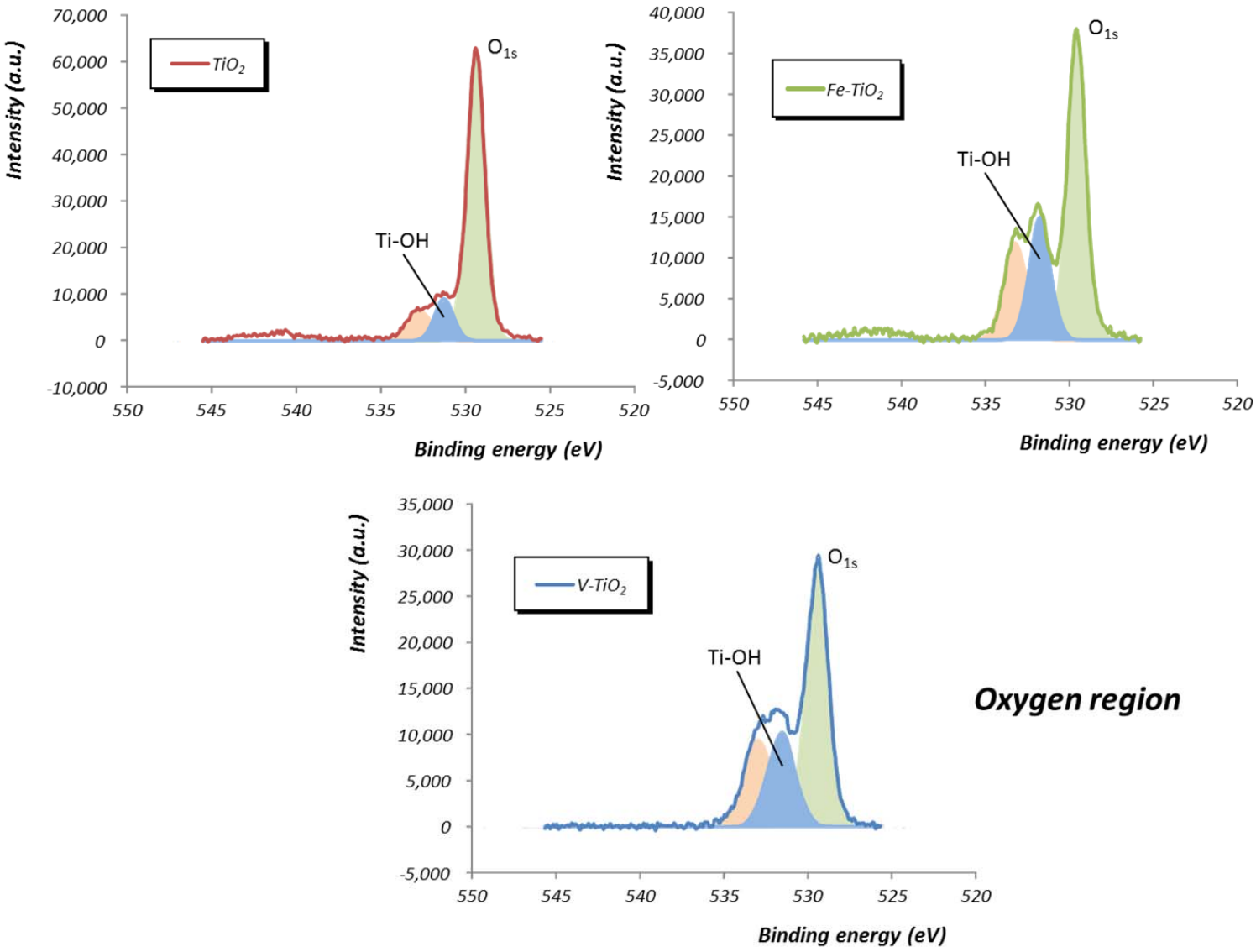

Figure 12. XPS results of the photocatalysts depicting the O region. Raw data from [73] have been processed to show the target region.

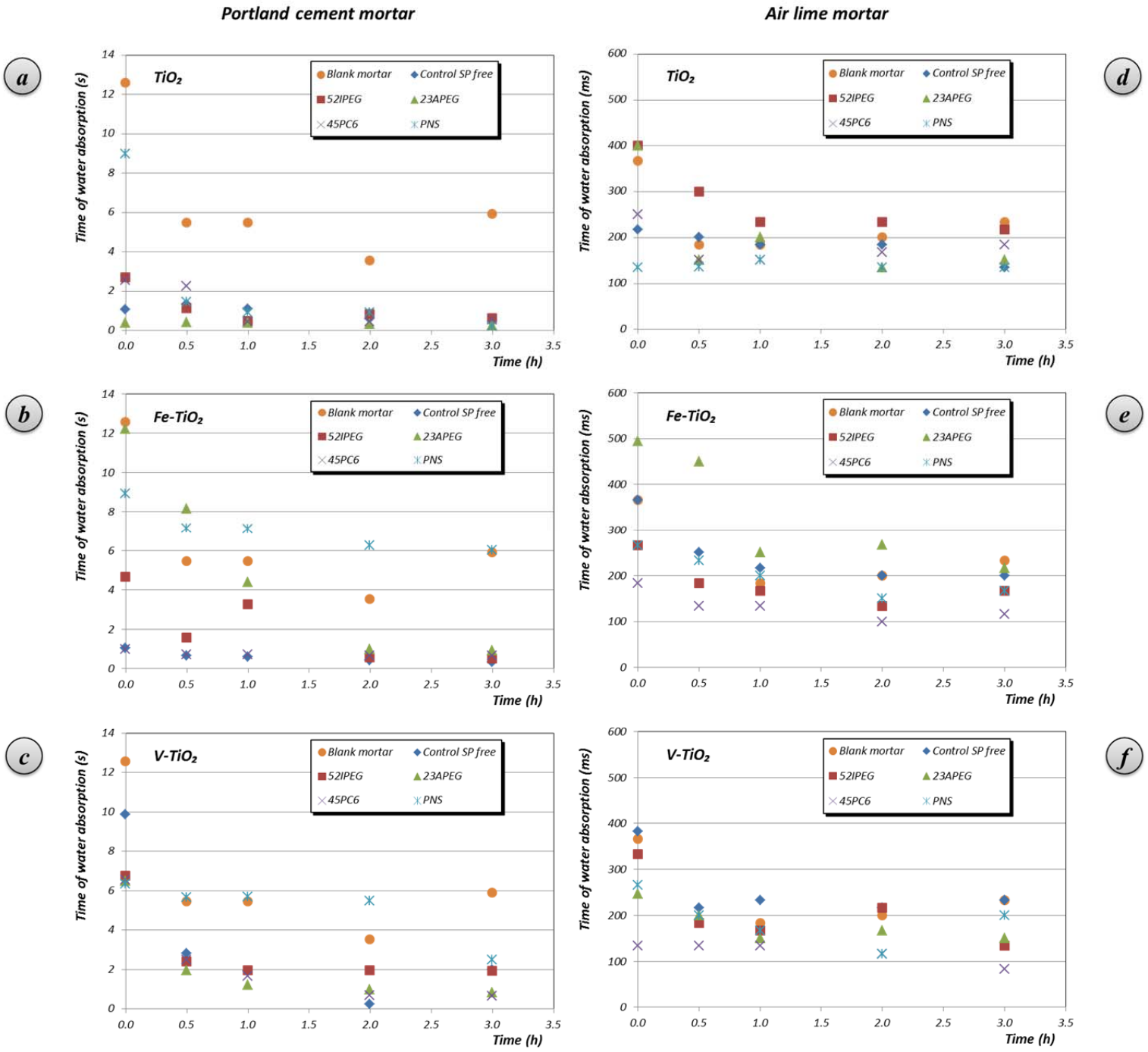

Figure 13. Time of water absorption in coatings applied onto Portland cement (a-c) and air lime (d-f) mortars under UV light exposition.

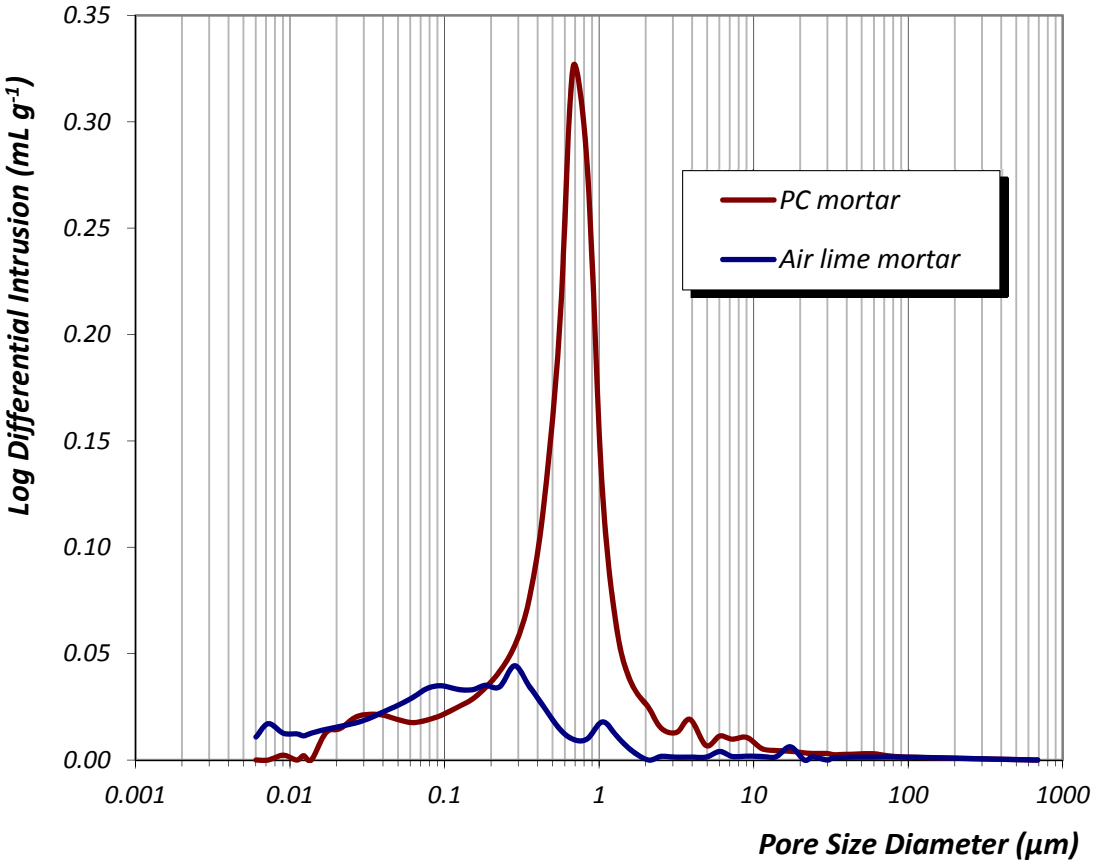

Figure 14. Pore size distributions of Portland and air lime mortars used as substrates.

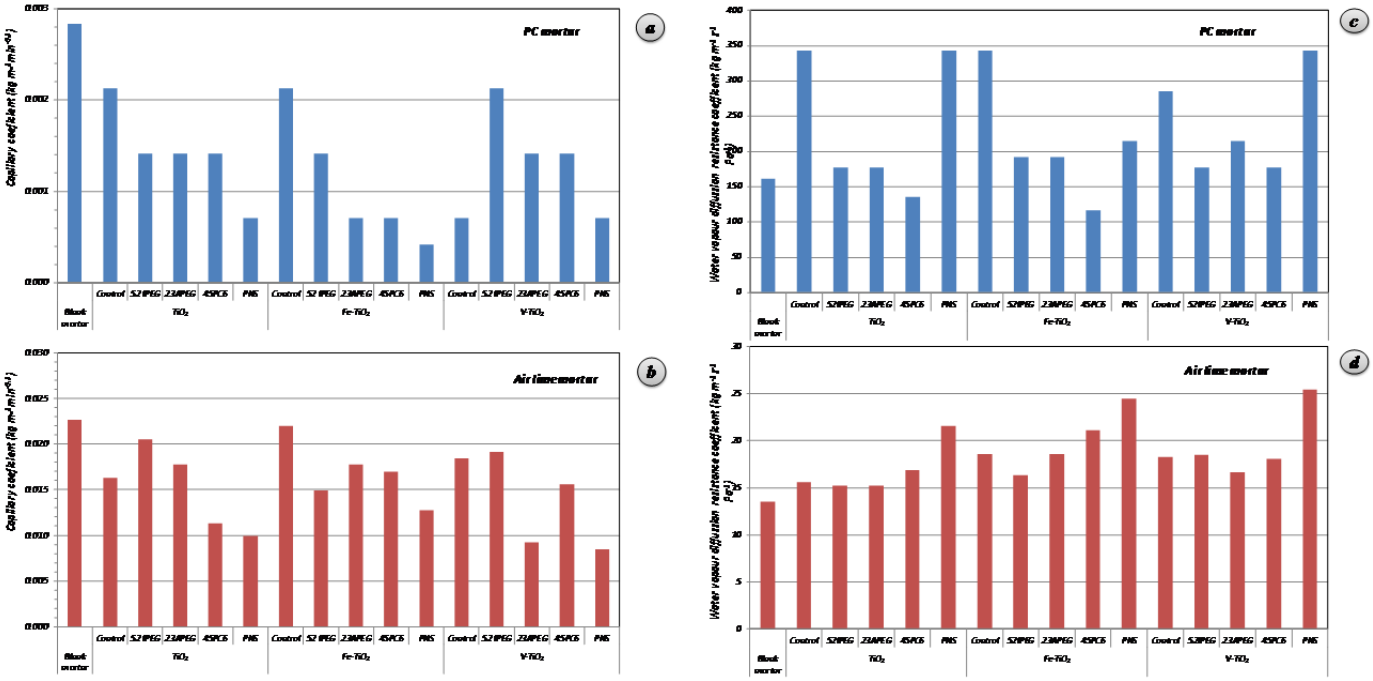

Figure 15. Capillary coefficient values and water vapour diffusion resistance coefficient values corresponding to different mortars: a) and c) Portland cement; b) and d) air lime mortars.

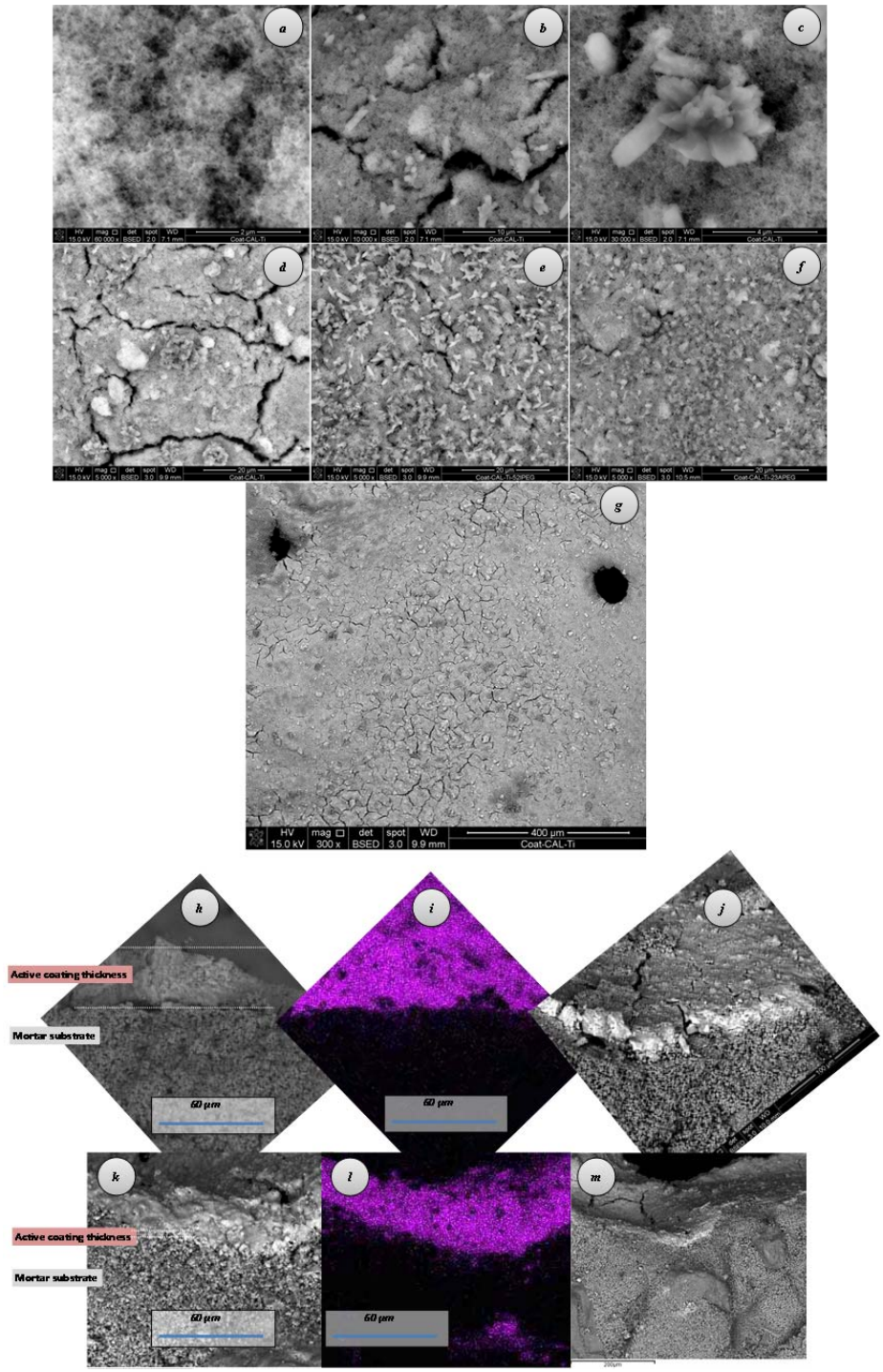

Figure 16. Microstructural SEM examination of bare TiO_2 coatings applied onto air lime mortars. Top view micrographs: a), b) c) and d) of control (SP-free) coating. e) Coating with 52IPEG. f) Coating with 23APEG. g) Mud cracking for control coating. Cross section micrographs: h), i) and j) of control (SP-free) coating. Elemental Ti mapping (EDS) is depicted in i). Cross section of coating with 52IPEG is shown in micrographs k), l) and m). Elemental Ti mapping (EDS) is depicted in l).

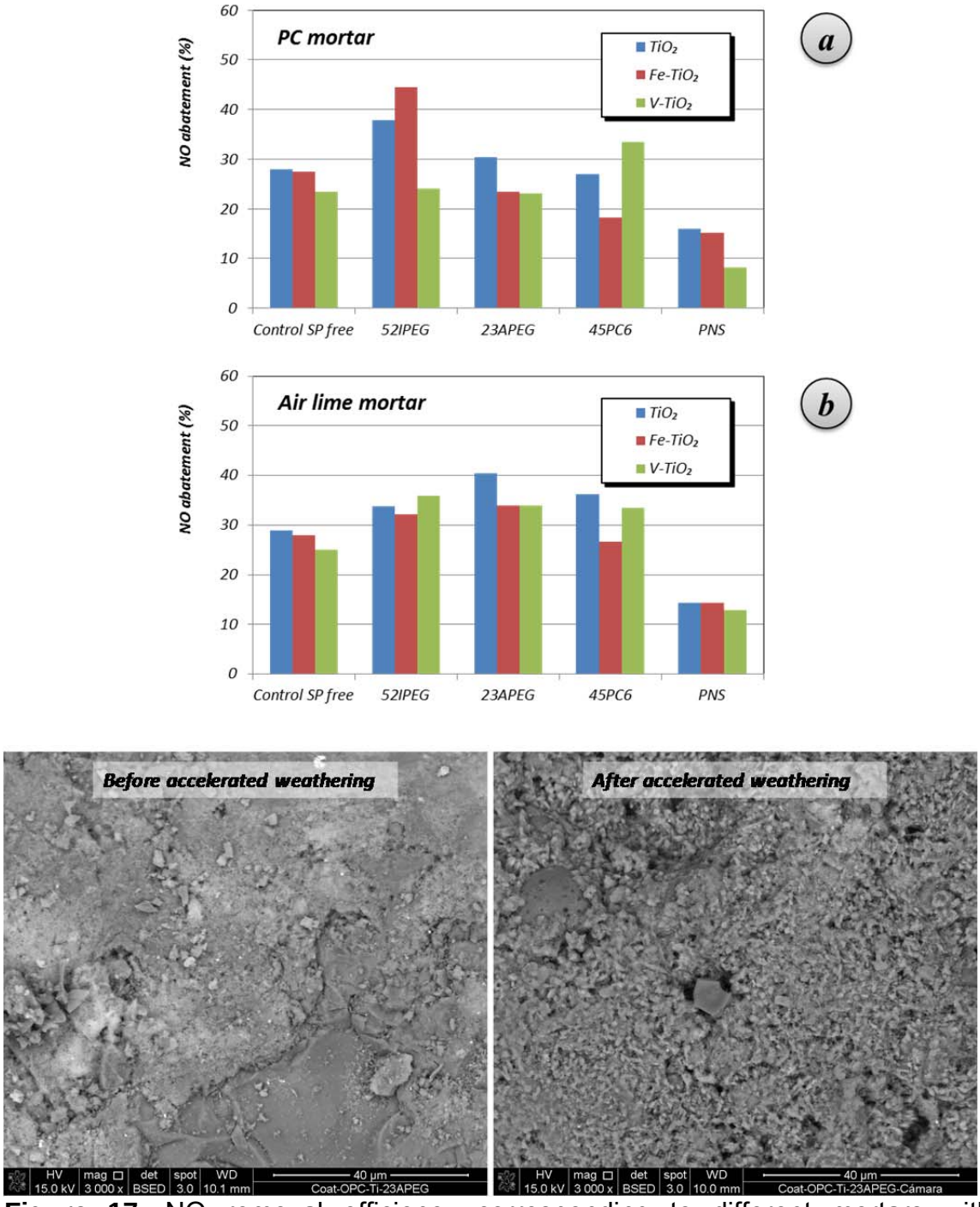

Figure 17. NO removal efficiency corresponding to different mortars with photocatalytic coatings after accelerated climatic ageing: a) Portland cement and b) air lime substrates. In the bottom part, SEM micrographs of PC mortar with TiO_2-23APEG coating before and after accelerated weathering.